CO_2 in the Surface Ocean FREE

Peter Landschützer, Max Planck Institute for Meteorology

https://doi.org/10.1093/acrefore/9780190228620.013.885
Published online: 21 June 2023

Summary

The global ocean comprises a significant sink for human-emitted carbon dioxide, yet many different processes are at play, causing strong spatial and temporal variations in the distribution of the sea surface pCO_2 and the resulting air-sea CO_2 fluxes. While dominated by the temperature-driven solubility, physical transport and biogeochemistry, the increase in the sea surface CO_2 partial pressure over the past decades is closely following the increase in atmospheric CO_2, resulting in a decreasing pH and decreasing saturation states of calcite and aragonite minerals. Despite the increasing abundance of novel data interpolation tools, e.g. based on machine learning, the heterogeneous distribution of CO_2 in the surface ocean requires a dense observing network to reconstruct global change.

Keywords: air–sea CO2 exchange, carbon dioxide, measurements, ocean, ocean acidification

Subjects: Climate Systems and Climate Dynamics

Processes driving CO_2 at the sea surface

Human activities such as fossil fuel burning and land use change have led to a significant increase in the atmospheric carbon dioxide (CO_2) concentration (Friedlingstein et al., 2022). Therefore, the exchange of carbon dioxide between the ocean and the atmosphere has become of primary interest, as the ocean comprises a major sink for human-made CO_2 (Gruber et al., 2019; Landschützer et al., 2014; Takahashi et al., 1993, 2009) removing 3.0 ± 0.4 Pg C/yr (Pg C/yr = petagramms of carbon per year, 1 Pg = 10^{15} g) in 2020 (Friedlingstein et al., 2022).

The uptake and release of carbon dioxide is tied to its concentration in the surface ocean and the overlying atmosphere. Due to the increasing concentration of carbon dioxide in the atmosphere and the resulting air-sea CO_2 gradient, the air–sea CO_2 exchange has become a primary research focus (Gruber et al., 2009; Landschützer et al., 2014; Takahashi et al., 2009).

Air–sea CO_2 exchange is driven by a concentration difference to its equilibrium concentration ($[CO_2,eq]$) and following Henry's Law, the equilibrium concentration in a liquid equals the solubility of a gas multiplied by the partial pressure of the gas above the liquid and is expressed as:

$$[CO_{2,eq}] = K_0 \; pCO_2 \tag{1}$$

Where K_0 describes the well-known temperature-driven gas solubility (Weiss et al., 1974).

The exchange of CO_2 at the air–sea interface can further be approximated using a simple two-layer model, or stagnant film model (Sarmiento & Gruber, 2006). In this two-layer model, the exchange of CO_2 is controlled by a small microlayer existing at the air–sea interface, both in the atmosphere and the ocean (Deacon, 1977; Jähne et al., 1987; Liss & Slater, 1974; Sarmiento & Gruber, 2006). Its thickness is determined by a turbulent surface layer on top of the microlayer. In the microlayer at the air–sea interface, diffusion is the dominant transport process, whereas away from the surface, turbulence becomes the dominant transport process for CO_2. The diffusive transport in the microlayer can be expressed by Fick's first law and simplified using finite differences to:

$$F_{micro} = -\epsilon \frac{\Delta \left[CO_2\right]}{\Delta z} \tag{2}$$

Where $\Delta[CO_2]$ is the concentration difference at the top and base of the respective microlayer, the diffusion coefficient can be expressed as:

$$\epsilon = k\, \Delta z \tag{3}$$

Where *k* is the kinematic gas transfer term through the respective microlayer. As proposed by Liss and Slater (1974), the transport of CO_2 in the air-sided microlayer (k_a) is orders of magnitude larger compared to the ocean microlayer (k_w) and can thus be ignored in further calculations.

Using this information, the exchange of CO_2 across the air–sea interface can be expressed by a simple bulk formulation and essentially be described by two controlling factors, namely the water-sided kinetic gas transfer velocity k_w, and the concentration gradient of CO_2 across the air–sea interface at the top of the respective microlayers (Sarmiento & Gruber, 2006) and takes the form:

$$\mathrm{F_{air–sea}} = \mathrm{kw}\ (\mathrm{[CO_{2,oc}]\text{-}[CO_{2,atm}]}) \tag{4}$$

The concentration difference is not always a practical measure for calculating the air-sea CO_2 flux. Hence, applying Equation (1), the flux can be expressed in terms of the partial pressure of CO_2, which is more applicable as it can be expressed from directly measurable quantities (Sarmiento & Gruber, 2006):

$$\mathrm{F_{air-sea}} = k_w \, \mathrm{K_0} \, \left(\mathrm{pCO_{2,oc}} - \mathrm{pCO_{2,atm}} \right) \tag{5}$$

Based on wind tunnel or field studies (see, e.g., Liss & Merlivat, 1986; Sweeney et al., 2007), many modeled estimates of the gas transfer velocity *k* emerged in the past decades being expressed as a function of the wind speed at 10 meters' height above surface. These range from linear (Liss & Merlivat, 1986), quadratic (Sweeney et al., 2007), over cubic (Wanninkhof & McGillis, 1999). Quadratic models have become the most-applied model for calculating the gas transfer across the air–sea interface from observations (see, e.g., Fay et al., 2021; Landschützer et al., 2013; Rödenbeck et al., 2013; Roobaert et al., 2018). Lastly, $pCO_{2,oc}$ and $pCO_{2,atm}$ describe the partial pressures of CO_2 in the ocean (subscript oc) and the atmosphere (subscript atm) in Equation (5), respectively.

While the kinetic gas transfer coefficient k_W (controlled by the surface winds) and the solubility K_0 (driven by the sea surface temperature) effect the magnitude of the air–sea CO_2 flux according to Equation (5), the pCO_2 gradient between the ocean and the atmosphere is responsible for both magnitude and the direction of the flux. Is the concentration or partial pressure of CO_2 lower at the sea surface than in the overlying atmosphere, the ocean will take up carbon dioxide from the atmosphere. Likewise, if the ocean partial pressure of CO_2 exceeds that of the overlying atmosphere, it will release CO_2 (see, e.g., Takahashi et al., 2002). As the pCO_2 in the ocean is varying significantly more than in the atmosphere (see, e.g., Takahashi et al., 2009), the partial pressure difference term is driven by the ocean in the absence of any local sources.

Besides the air–sea interface, the ocean–land boundary plays another important role in the transfer of carbon dioxide in surface waters. Land-to-ocean transport through the land-to-ocean-aquatic continuum (LOAC), i.e., inland waters, estuaries, tidal wetlands, and continental shelf waters, is a major source of marine carbon (Regnier et al., 2013) in the form of dissolved inorganic and organic carbon as well as particulate organic carbon (POC). Regnier et al. (2022) suggest two major mechanistic short-range loops connected by a long-range loop being in place that direct the LOAC transport of carbon. Through a first loop, carbon from terra firme ecosystems enters inland waters of which the majority of the carbon evades back to the atmosphere. A fraction of the inland water carbon (excluding a fraction subject to burial along the way), however, is transported further in a long-range loop to tidal wetlands, estuaries and eventually continental shelf water where it enters the second short-range loop, the air–sea exchange loop.

The distribution of the partial pressure of carbon dioxide in the surface ocean follows a complex pattern (Landschützer et al., 2014; Takahashi et al., 2002, 2009). This is illustrated in Figure 1, which stems from the reconstruction of surface ocean measurements collated within the SeaFlux dataset (Fay et al., 2021), including open oceans (Chau et al., 2020; Denvil-Sommer et al., 2019; Gregor et al., 2019; Iida et al., 2020; Landschützer et al., 2016; Rödenbeck et al., 2013; Zeng et al., 2014) and coastal oceans (Landschützer et al., 2020; Laruelle et al., 2017), and illustrates the decadal mean partial pressure and air–sea CO_2 flux density from 2010 to 2019. The figure already

reveals several hotspots for carbon dioxide in the surface ocean such as the equatorial Pacific and coastal zones, whereas the high-latitude northern hemisphere as well as the mid-latitude southern hemisphere reveal the lowest partial pressures of CO_2. As a consequence, most regions globally illustrate marine sink regions for atmospheric CO_2.

Little variation can be observed in the pCO_2, delta pCO_2, and air–sea CO_2 flux density looking at the meridional median pCO_2 in Figure 1, ranging between 350 and 380 µatm, -30 and 0 µatm, and -1 to 0 mol m^{-2} yr^{-1}, respectively. Most of the variations observed can be linked to the distribution of land masses, and linked to that, the presence of marginal seas, such as the Mediterranean Sea or the Labrador Sea. Therefore, the observed east–west variations are largely the result of the spatial extent of the ocean.

A much more diverse picture evolves looking at the zonal median pCO_2 in Figure 1, with substantial differences in the sea surface pCO_2 between the equator—exceeding 400 µatm—and the poles—below 340 µatm in the Arctic Ocean. The similarity between the partial pressures of CO_2 and the partial pressure difference reveals that the surface ocean is the driving force of the spatial air–sea CO_2 flux variations,(Landschützer et al., 2014; Takahashi et al., 2002, 2009). Consequently, the equatorial ocean is a source of carbon dioxide to the atmosphere and the high-latitude ocean—with the exception ossf the Southern Ocean south of the Polar front—is a strong sink of carbon dioxide from the atmosphere. In the Arctic Ocean, strong pCO_2 gradients do not result in strong air–sea CO_2 fluxes due to the presence of sea ice blocking the physical transfer across the air–sea interface. Hence, in order to account for the effect of sea ice on the air–sea CO_2 flux, Equation (5) is usually expanded to

$$\mathrm{F_{air\text{–}sea}} = k_w \, \mathrm{K_0} \, \left(\mathrm{pCO_{2,o}} - \mathrm{pCO_{2,a}}\right) (1 - \mathrm{SI}) \tag{6}$$

where SI represents the sea-ice fraction. According this simplified equation, no air–sea mass exchange takes place if the ocean is fully covered by seaice.

The low latitude maximum in Figure 1 can be largely explained by the high pCO_2 partial pressure in the equatorial Pacific and to a lesser degree in the Atlantic and Indian Ocean sectors. The zonal median steadily shows a decrease in pCO_2 poleward and does not indicate a strong relation with land masses, with the exception north of 60° N where a sharp drop in CO_2 can be observed. In the Southern Ocean, the sea surface pCO_2 increases again south of 40° S.

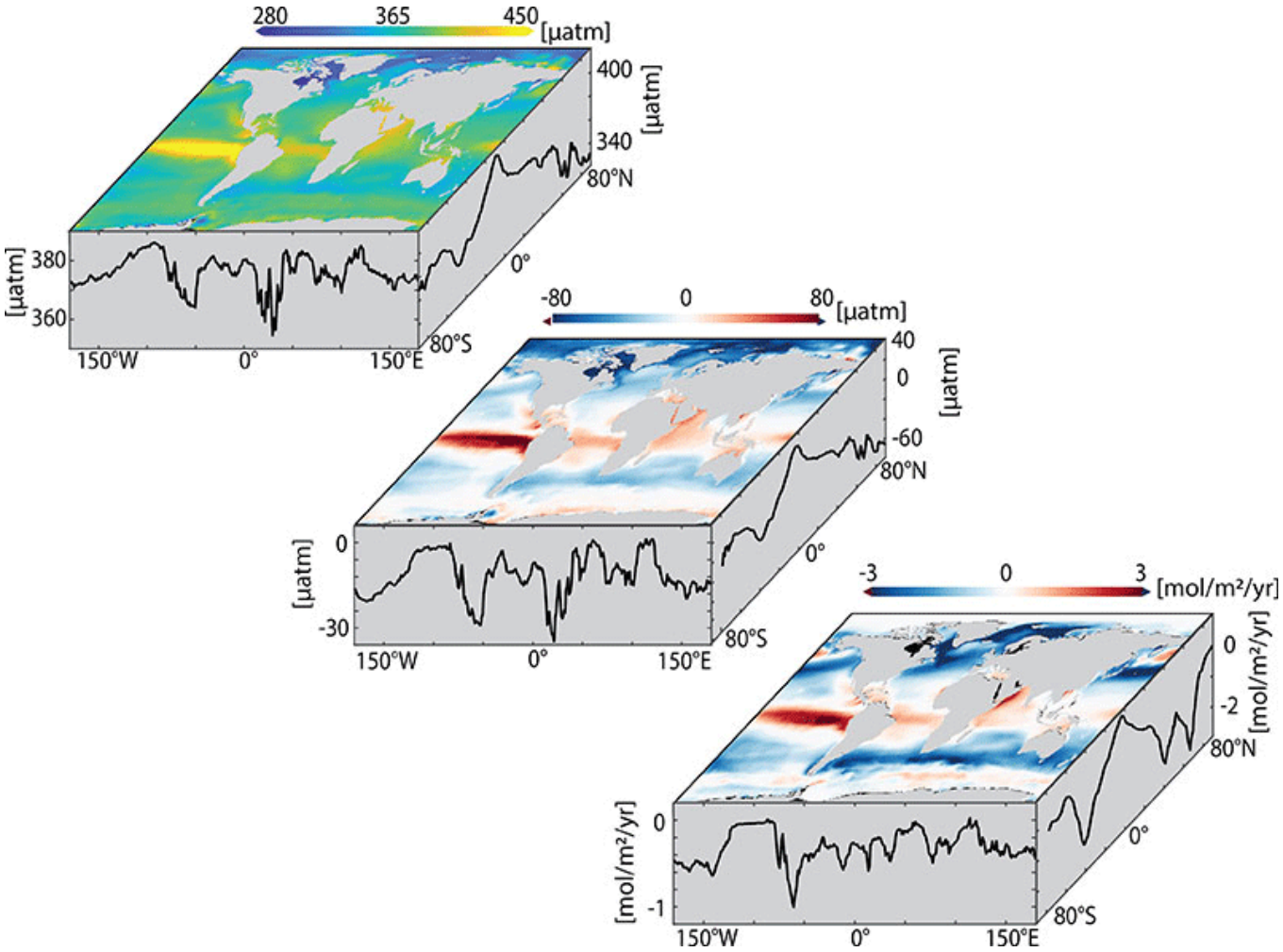

Figure 1. Mean sea surface partial pressure of CO_2 (pCO_2, left), delta pCO_2 (middle) and air–sea CO_2 flux (right) from 2010 to 2019 as a map in the center as well as its zonal and meridional median variation. Atmospheric pCO_2 is calculated from the dry molar fraction (xCO_2; Dlugokencky & Tans, 2018) at sea level pressure (Kalnay et al., 1996) assuming 100% humidity at the air-sea interface (Dickson et al., 2007).

Source: Author.

At first glance at the distribution of the partial pressure of CO_2 in the surface ocean already reveals the importance of the north–south picture compared to the the east–west picture. The complex distribution of CO_2 in the ocean illustrated in Figure 1 is the result of many regional drivers acting on the carbonate system and is the result of the interplay of several partly competing mechanisms, e.g., as illustrated in Figure 2. The exchange of CO_2 between the ocean at the air–sea and land–sea interfaces, as well as biological uptake of dissolved carbon and physical transport between the surface and the deep ocean, are among the main contributors (see, e.g., Sarmiento & Gruber, 2006).

Gaseous CO_2 entering the ocean via the air–sea interface dissolves in seawater forming carbonic acid (H_2CO_3), bicarbonate (HCO_3^-) and carbonate ions (CO_3^{2-}), collectively referred to as dissolved inorganic carbon (DIC), i.e., a massive carbon pool in the ocean accounting for a total of about 37,000 Pg C (Keppler et al., 2020). These reactions are summarized following Millero et al 2013, Zeebe and Wolf-Gladrow (2001) and Sarmiento and Gruber (2006):

$$\mathrm{CO_{2(gas)} + H_2O \rightleftharpoons H_2CO^*_3} \tag{7}$$

$$\mathrm{H_2CO^*_3 \rightleftharpoons H^+ + HCO_3^-} \tag{8}$$

$$\mathrm{HCO_3^- \rightleftharpoons H^+ + CO_3^{2-}} \tag{9}$$

where:

$$[\mathrm{H_2\ CO_3^*}] = \left[\mathrm{CO_{2(w)}}\right] + [\mathrm{H_2\ CO_3}] \tag{10}$$

The sum of the products formed by these reactions is the total DIC concentration:

$$[\mathrm{DIC}] = [\mathrm{H_2\ CO_3^*}] + \left[\mathrm{HCO_3^-}\right] + \left[\mathrm{CO_3^{2-}}\right] \tag{11}$$

and the equilibrium relationships of these are:

$$K_0 = \frac{[\mathrm{H_2\ CO_3^*}]}{p\,\mathrm{CO_2}} \tag{12}$$

$$K_1 = \left[\mathrm{HCO_3^-}\right]\left[\mathrm{H^+}\right] / [\mathrm{H_2\ CO_3^*}] \tag{13}$$

$$K_2 = \left[\mathrm{CO_3^{2-}}\right]\left[\mathrm{H^+}\right] / \left[\mathrm{HCO_3^-}\right] \tag{14}$$

where K_0 describes the CO_2 solubility. Only a small fraction remains as CO_2, with the solubility being the controlling factor of the dissolution (Sarmiento & Gruber, 2006; Weiss, 1974). Therefore, the sea surface temperature plays an major role regarding the distribution of pCO_2 at the sea surface (see Figure 3). One additional important parameter to determine the carbon system in the ocean is total alkalinity (TA), defined by Dickson and Goyet (1994) as:

$$\mathrm{TA} = \left[\mathrm{HCO_3^-}\right] + 2\left[\mathrm{CO_3^{2-}}\right] + — \left[\mathrm{H^+}\right] + \left[\mathrm{B(OH)_4^-}\right] + \text{minor contributions} \tag{15}$$

Based on these reactions, the sea surface pCO_2 can be described as a function of the reaction products and their equilibrium constants, as well as approximations of the DIC and TALK concentrations (see, e.g., Sarmiento & Gruber, 2006):

$$\mathrm{pCO_{2(w)}} = \frac{K_2}{K_0 K_1} \frac{\left[\mathrm{HCO_3^-}\right]^2}{\left[\mathrm{CO_3^{2-}}\right]} \approx \frac{K_2}{K_0 K_1} \frac{(2[\mathrm{DIC}] - [\mathrm{TA}])^2}{[\mathrm{TA}] - [\mathrm{DIC}]} \tag{16}$$

Thus, the surface pCO_2 is affected by the ratio of the equilibrium constants and the DIC and the TA concentration of the seawater. While the equilibrium constants are determined by the sea surface temperature and salinity, the DIC concentration is influenced by the exchange of CO_2 with the atmosphere, and both DIC and TALK are influenced by biological processes and physical mixing (Sarmiento & Gruber, 2006). $\mathrm{H^+}$

The sea surface temperature pattern is closely tied to the radiation balance of the Earth's surface and in particular the incoming solar shortwave radiation (Talley et al., 2011). In cold waters, more CO_2 dissolves than in warm waters and a decrease in temperature lowers the CO_2 partial pressure in the surface ocean, leading to waters to become undersaturated with regard to atmospheric CO_2, and vice versa for an increase in temperature. Thus, a temperature decrease between the warm tropics and the cold high latitudes in part explains the zonal pCo_2 gradient identified in Figure 1. The solubility driven control on the surface ocean pCO_2 in combination with physical carbon sequestration in and from the interior ocean through ventilation is often referred to as solubility pump (see Figure 2).

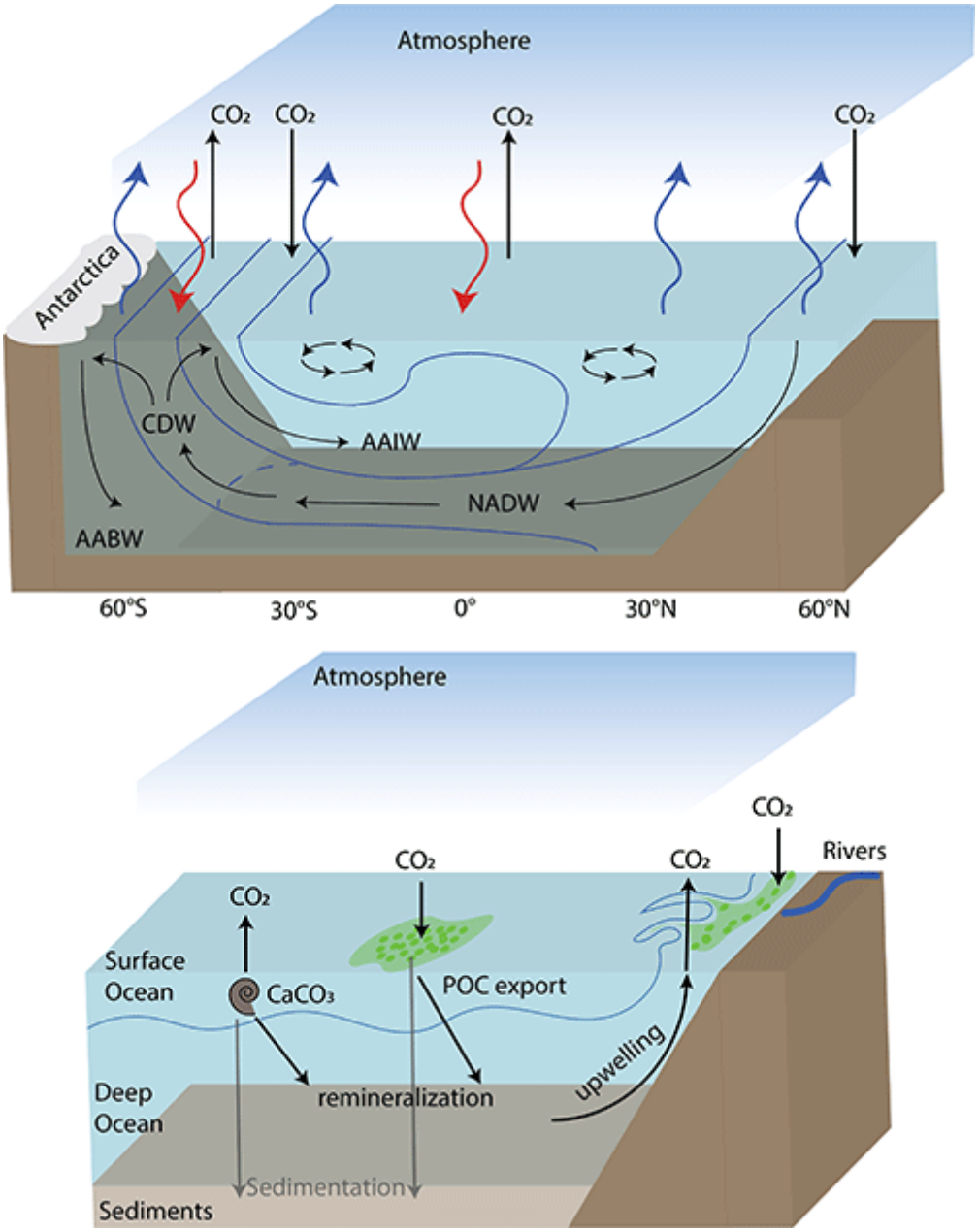

Figure 2. (Top) Illustration of the solubility pump following Marshall and Speer (2012) and Sarmiento and Gruber (2006) using an Atlantic Ocean crosssection, where major pathways for CO_2 (black arrows) from the surface to the interior and back are indicated with associated heat gain and loss (I.e. buoyancy gain and loss in red and blue arrows). Abbreviations indicate major water masses, i.e., North Atlantic Deep Water (NADW), Antarctic Bottom Water (AABW), Circumpolar Deep Water (CDW) and Antarctic Intermediate Water (AAIW). (Bottom) Illustration of the biological carbon pumps. CO_2 at the surface is consumed by primary producers and exported to the deep ocean as particulate organic carbon (POC). In contrast, calcium carbonate produced at the sea surface releases CO_2. Organic carbon exported to the deep gets remineralized and brought back to the euphotic zone, e.g., through physical mixing at the coast.

Source: Author.

Dissolved inorganic carbon is distributed like a passive tracer (Heinze et al., 2015) throughout the water column, such as through intermediate and deep-water formation, and is stored in the deep ocean up to several centuries until it resurfaces (Gruber et al., 2009; Sarmiento & Gruber, 2006). Physical transport, deep-water ventilation, and the wind-induced physical mixing, therefore, significantly contribute to the observed north-to-south pCO_2 pattern (Gray et al., 2018; Gruber et al., 2009). This is evident, for example, in a latitude band between 40° and 60°, where warm subtropical waters that are transported poleward mix with cold and nutrient-rich subpolar waters, drawing down the pCO_2 on the one hand through cooling, and on the other hand through biological production (Takahashi et al., 2002).

In contrast, Ekman driven upwelling in the tropical Pacific (Feely et al., 2006) fueled by the trade winds, or in the Southern Ocean (Frölicher et al., 2015) fueled by the westerlies is responsible for the regional high pCO_2 in surface waters. The same can be seen in upwelling regions, where the upwelling of carbon-rich waters in the Eastern Boundary Upwelling Systems leads to the resurfacing of CO_2 (Franco et al., 2018; Lovecchio et al., 2018) 1.

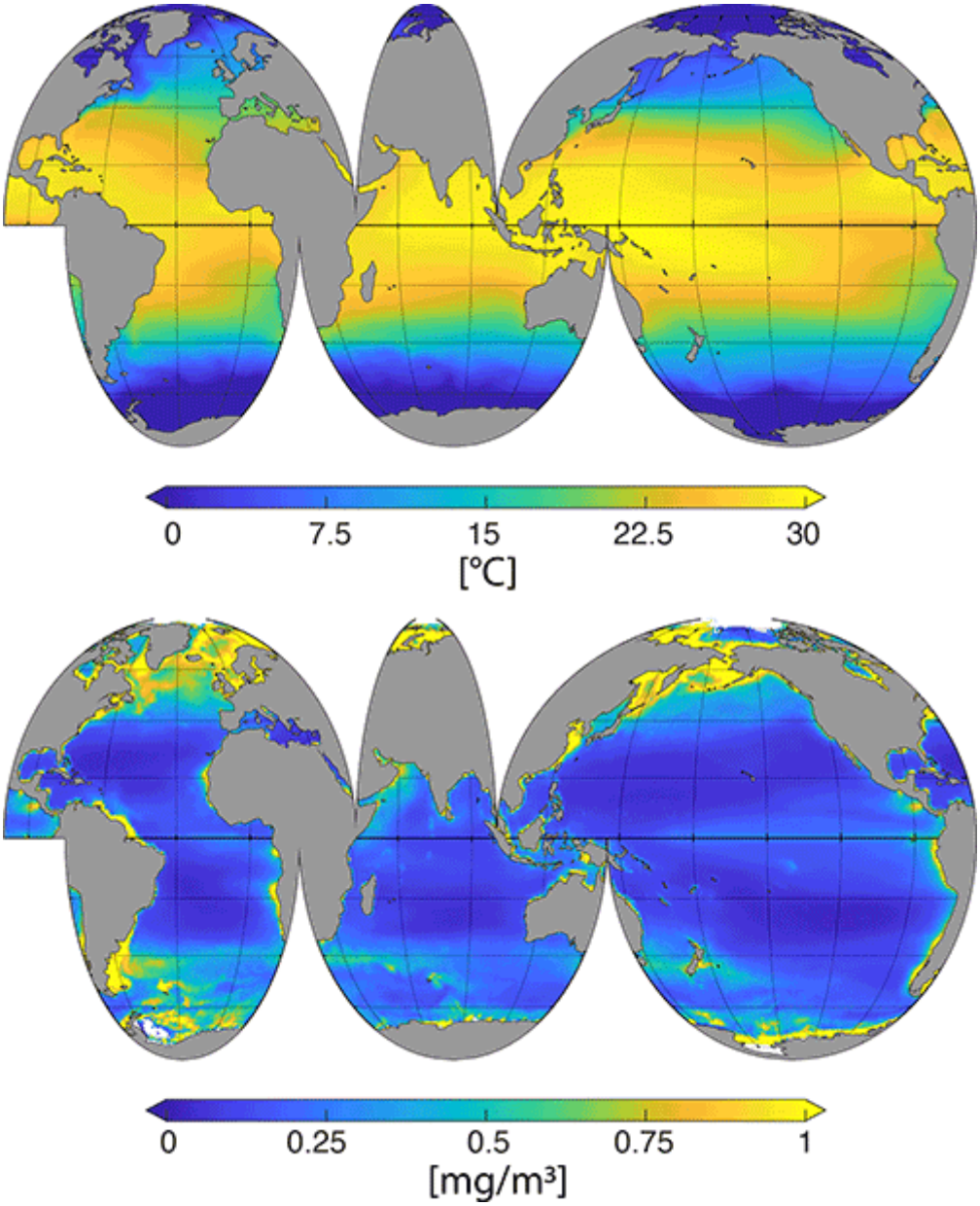

Figure 3. Decadal mean distribution of sea surface temperature (Reynolds et al., 2002) and chlorophyll-a (Maritorena et al., 2010, Globcolor project: www.globcolour.info <http://www.globcolour.info>) as proxy for biological production from 2010 to 2020.

Source: Author.

While the solubility pump alone causes only a small gradient between the surface DIC and the interior DIC, the largest vertical gradients in DIC are driven by biology (Heinze et al., 2015; Sarmiento & Gruber, 2006). Primary producers, and in particular phytoplankton, consume dissolved CO_2 during their photosynthetic energy production forming organic carbon. The seasonal carbon drawdown linked to net community production is estimated to be 8.2 ± 5.6 Pg C/yr (Keppler et al., 2020). An indication where biological production is particularly strong can be

obtained from ocean color measurements as illustrated in Figure 3 showing the concentration of chlorophyll-a (Maritorena et al., 2010; Globcolor project: www.globcolour.info <http://www.globcolour.info>) in the sea surface as a proxy for primary production.

Biomass formed by primary producers is then transferred to higher trophic levels through grazing. A fraction of particulate matter forming at the surface is then exported as POC to the deeper ocean layers through sinking, fecal pallets, and other means (see, e.g., Henson et al., 2011; Le Moigne, 2019). The majority of the exported carbon is later remineralizer and brought back to dissolved phase within the upper 1500 m (Heinze et al., 2015), whereas sedimentation of organic carbon provides a natural pathway to sequester carbon.

This transport of organic carbon from the surface below the mixed layer as well as its remineralization is then referred to as biological carbon pump. Light and nutrient availability as well as other environmental conditions control the strength of the biological carbon pump (Heinze et al., 2015). Figure 3 reveals localized maximalinked to coastal systems and shelve seas, where river systems or coastal upwelling supplies nutrients for primary producers (Dai et al., 2022).

A second important mechanism linked to biology is the calcium carbonate counter pump following the equation:

$$\mathrm{Ca^{2+} + 2\,HCO_3^- \rightleftharpoons CaCO_3 + CO_2 + H_2O} \tag{17}$$

During the shell-building process of marine biota, $\mathrm{HCO_3^-}$ is converted to $\mathrm{CO_3^{2-}}$ and CO_2 is released to the seawater. $CaCO_3$ occurs either as aragonite or calcite and is further discussed in the section "Impacts of a Changing Carbon Cycle." Upon death of calcifying organisms, they sink through the water column where a large fraction is remineralized in the water column or the sediment. The effect of the $CaCO_3$ counter pump, is small compared to the POC driven pump, and does not fully compensate the CO_2 drawdown by biology (Heinze et al 2015).

One of the challenges untangling the mechanisms driving the sea surface pCO_2 pattern and the resulting air–sea CO_2 flux, is that they are of competing nature. Upwelling of deep waters on the one hand leads to resurfacing and warming of carbon-rich deep waters and a subsequent increase in the sea surface pCO_2. On the contrary, resurfaced nutrients stimulate biological production consuming carbon (see Figure 2). One simple concept to separate the driving mechanisms is to isolate the temperature effect on the dissolution of CO_2 in seawater. Based on idealized laboratory experiments, Takahashi et al. (1993) found that the effect of temperature on the pCO_2 can be expressed by:

$$\left(\partial \mathrm{pCO_2}/\partial \mathrm{T}\right)/\mathrm{pCO_2} = 0.0423\,^{\circ}\mathrm{C}^{-1} \tag{18}$$

Based on this simple concept, the driving mechanisms of the sea surface pCO_2 can be simply divided by contributions from temperature and those driven by non-thermal contributors (i.e., the biological pump, circulation, etc. - see also Takahashi et al 2002). Surprisingly, this simple separation reveals remarkably uniform zonal boundaries at least for the seasonal cycle and its change in time (Landschützer et al., 2018; Takahashi et al., 2002). Poleward of about 40° N and 40° S, the non-thermal component dominates the seasonal variations in the sea surface pCO_2, whereas in a narrower band between 20° and 40° S and 20° and 40° N, the solubility dominates the seasonal pCO_2 variability.

Surface Ocean CO_2 Measurements

Based on the bulk formulation presented in Equation (5), sea surface temperature, wind, and atmospheric pCO_2 as well as sea surface ocean pCO_2 are the essential measurements to track the fate of the ocean carbon sink.

The challenge this method faces is data sparsity (Bakker et al., 2016) and uncertainties related to the kinematic transfer across the air–sea interface (Jähne et al., 1987; Roobaert et al., 2018; Wanninkhof 1992). While atmospheric CO_2 is well mixed, varying by a few μatm around the globe spatially, it can be sufficiently constrained for air–sea CO_2 flux calculations by few measurement stations. In the ocean surface, however, the pCO_2 can vary spatially by several hundreds of μatm (Takahashi et al., 2009), that is, up to 2 orders of magnitude larger than in the atmosphere.

These strong variations evident from Figure 1 and linked to the processes in Figure 2 require an understanding of the variations in the sea surface pCO_2, i.e., the component dominating the direction of the air–sea CO_2 exchange. Therefore, a dense observing network needs to be in place to observe the sea surface pCO_2 and air–sea CO_2 exchange.

Measuring a gas dissolving in seawater is challenging. Current state-of-the-art measurement systems for the sea surface pCO_2 operating on ships are built on equilibration systems (see, e.g., Cooper et al., 1998; Körtzinger et al., 1996). Seawater pumped through an inlet is brought in contact with a small isolated air volume in an equilibrator. These equilibrators are built in such a way that the air–water interface is large and the exchange of CO_2 between the seawater and the air volume is rapid, so that the small air volume quickly equilibrates with the water provided through the seawater inlet (i.e., the ships' seawater supply). Through infrared absorption, the amount of CO_2 in the air volume can be precisely measured, and through standard corrections (Dickson et al., 2007; Pierrot et al., 2009), the seawater pCO_2 can be obtained. These systems are highly accurate and uncertainties are largely within 2 μatm for the most reliable systems in place (Bakker et al., 2014, 2016; Pfeil et al., 2013). To maintain that high accuracy, however, these systems require regular maintenance, calibration, and intercomparison (see, e.g., Körtzinger et al., 1996). Furthermore, recent literature suggests that the instrument setup, with seawater inlets at depth of 5-10 meters below the sea surface, requires additional correction for temperature gradients between the actual instrument and the sea surface skin layer (Woolf et al., 2016), in order to reconstruct the air–sea CO_2 exchange (Watson et al., 2020).

Though data collection efforts and community synthesis efforts collating measurements in large databases (Bakker et al., 2014, 2016; Pfeil et al., 2013; Takahashi et al., 2019), the number of available measurements has significantly increased in recent years. The Surface Ocean CO_2 Atlas (SOCAT; Bakker et al., 2016) included in its first release in 2011 around 7 million measurements (a similar number of measurements was also collected within the LDEO database; Takahashi et al., 2019). In its 2021 release, the SOCAT database already included over 30 million measurements, i.e., a fourfold increase. Figure 4 shows the available measurements from 1980 onward.

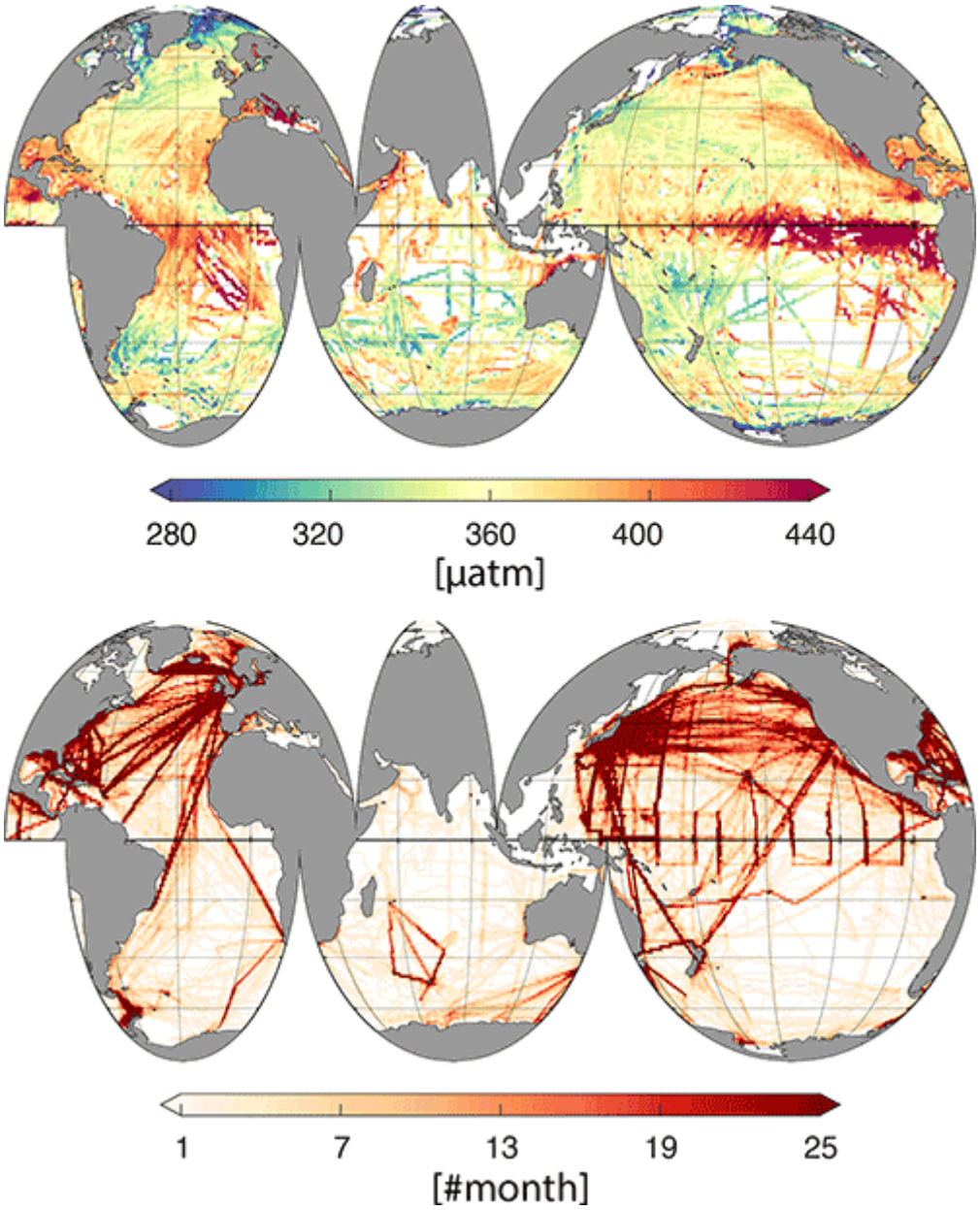

Figure 4. Top: Measurements of the sea surface pCO_2 from 1980 onward in the SOCATv2020 database (Bakker et al., 2016). Bottom number of occupied pixels with at least one pCO_2 measurement region within the SOCAT database since 1980.

Source: Author.

Despite the incredible community effort, Figure 4 illustrates the substantial difference in the pCO_2 coverage between the hemispheres. In the southern hemisphere, large ocean regions still remain unobserved, e.g., the southeast Pacific Ocean. The challenge seems obvious: The size of the ocean covering 71% of the planet's surface, the rough conditions, and the remoteness of some ocean regions provide a challenge in observing these regions.

The relatively good coverage in the northern hemisphere is in part the result of the valuable partnership between scientists and industry through the Ships of Opportunity program network (see, e.g., Cooper et al., 1998; Körtzinger et al., 1996). Within this network, cargo and other ships are equipped with instruments to measure the sea surface pCO_2 during their regular ocean crossings. This partnership has led to a step-change in understanding the marine carbonate system in the northern hemisphere, where the majority of industrial shipping lines operate, easily visible in Figure 4.

The missing measurements and their missing representation over time in the southern hemisphere (see Figure 4) is problematic, given that the Southern Ocean south of 35° S is the most important marine sink for human-made CO_2 having absorbed nearly 40% of all the ocean CO_2 since industrialization (Frölicher et al., 2015). Additionally, 75% of the excess heat from greenhouse warming is observed in this remote ocean region.

In response to this lack of shipboard sea surface pCO_2 measurements in the southern hemisphere, scientists have started to develop new sensor technology to fill this gap. Since 2014, as part of the Southern Ocean Carbon Observations and Modelling project, autonomous biogeochemical floats equipped with biogeochemical sensors have been continuously deployed in the Southern Ocean region (Gray et al., 2018; Williams et al., 2017). Unlike the equilibrator systems on ships, floats do not measure the pCO_2 directly, but instead temperature, salinity (from which total alkalinity is calculated), and pH. Using carbonate system calculations (Humphreys et al., 2022; Lewis & Wallace, 1998; van Heuven et al., 2011), the sea surface CO_2 can be deprived, though with larger uncertainty of ±2.86% of the reading suggested by Bushinsky et al. (2019).

Other, less numerous but accurate autonomously navigating pCO_2 measurement devices to fill the data void include saildrones (Sutton et al., 2021). Unlike floats, saildrones remain at the ocean surface and directly measure the pCO_2 on a predefined route. Withstanding the harshest ocean conditions, these saildrones have already completed a full circumnavigation of Antarctica, continually measuring pCO_2 (Sutton et al., 2021). Another alternative platform to fill the Southern Ocean data void in the future are sailboats. While size, weight, and energy consumption of CO_2 measuring systems has historically been a challenge for sailboats, the latest membrane sensor development (see, e.g., Arruda et al, 2020) has led to the reduction of size weight and energy consumption of equilibrator systems offering the opportunity to be deployed on smaller vessels. Unlike the classical equilibrator systems (see, e.g., Cooper et al., 1998), the equilibration of seawater and the air volume that is then analyzed via infrared absorption occurs through a membrane. While being further developed, these systems mounted on sailboats during round-the-globe racing events have already supplied essential data from the southern hemisphere for the analysis of the air–sea CO_2 exchange Friedlingstein et al., 2022

Reconstructing the Air–Sea CO_2 Exchange

Given the importance of the ocean in absorbing greenhouse gases such as CO_2, a lot of emphasis has been placed on measuring and monitoring the air–sea CO_2 exchange. Currently the ocean CO_2 sink is monitored based on measurements of the dissolved inorganic carbon content (Gruber et al., 2019; Khatiwala et al., 2013; Olsen et al., 2019; Sabine et al., 2004), atmospheric ratios of the N_2/O_2 content (Manning & Keeling, 2006), or chlorofluorocarbon penetration time scales (McNeil et al., 2003). These highly accurate estimates provide a snapshot view of the mean rate at which the ocean absorbs carbon dioxide. Variations on seasonal over interannual through decadal timescales, however, cannot be constrained with these respective methods. A more recent alternative is provided by atmospheric CO_2 measurements and an approach where the transport of CO_2 is inverted and can be tracked back to its sources and sinks (e.g., Rödenbeck et al., 2003). The caveat, however, is that these methods have difficulties separating air–land and air–sea fluxes and their variability is dominated by the land fluxes.

Ocean process models run in hindcast mode—that is, forced with historical atmospheric conditions—have been historically used to constraining the ocean CO_2 sink and its variability in time (Friedlingstein et al., 2022). While the models suggest significant local variability in the air–sea CO_2 flux, e.g., driven by El Niño Southern Oscillation in the equatorial Pacific, the long-term trends closely follow the expected increase due to the rise in atmospheric CO_2, with little variations around this increase (DeVries et al., 2019; Gruber, Landschützer, & Lovenduski, 2019).

With the increasing number of sea surface pCO_2 measurements, air–sea CO_2 flux estimates based on the bulk transfer method (Equation (5)) started to evolve. The main challenge these methods face, however, is linked to the data sparsity evident from Figure 4. But even in the northern hemisphere, no full pCO_2 coverage exists on yearly or even shorter timescales, hence some form of data interpolation method is required, particularly, as global autocorrelation length scales of measurements are in the order of 400 km (Jones et al., 2012). Therefore, in parallel with the increasing number of measurements, several data interpolation methods, such as those based on nonlinear regression methods, and machine learning tools evolved (Gregor et al., 2019; Landschützer et al., 2016; Ritter et al., 2017; Rödenbeck et al., 2015; Sommer-Denvil et al., 2019; Zeng et al., 2014). While in the early and mid-2000s a climatological mean estimate of the air–sea CO_2 exchange based on marine pCO_2 measurements existed (Takahashi et al., 2002, 2009), there are at present multiple estimates covering decadal timescales at monthly resolution (Friedlingstein et al., 2022; Rödenbeck et al., 2015). Most recently, with the development of the SeaFlux dataset, a first unified ensemble of these estimates has been released (Fay et al., 2021).

One remarkable finding of these newly evolving methods was the substantially larger variations in the air–sea CO_2 flux (DeVries et al., 2019) than previously recognized, driven by the sea surface partial pressure of CO_2 (Landschützer et al., 2015). Particularly in the data-sparse Southern Ocean, discrepancies emerged in the representation of interannual through decadal air–sea CO_2 flux variations between different air–sea CO_2 flux estimates (DeVries et al., 2019; Gruber, Landschützer, & Lovenduski, 2019; Hauck et al., 2020), raising the question as to what extent these basin-wide variations are just an artifact of the observed local variations from local well-observed Southern Ocean regions (Munro et al., 2015; Xue et al., 2015). This has further been

indicated by studies by Bushinsky et al. (2019), Gray et al. (2018), and Gloege et al. (2021), showing that data sparsity is still the main source of uncertainty in reconstructing basin-wide sea surface pCO_2 maps from observations, with uncertainties in the air–sea exchange ranging from 20% to 40% depending on the ocean basin. Additionally, uncertainties in the gas transfer and the different wind reanalysis products have been shown to add an additional 20% to the air–sea CO_2 fluxuncertainty (Roobaert et al., 2018).

pCO_2 Variations in Time

The processes controlling the partial pressure of CO_2 in the surface ocean vary on multiple timescales. In a steady state view, for example pre-industrial conditions with steady climate and no external sources or sinks of CO_2 (such as input of CO_2 from rivers or loss through sedimentation), the atmosphere and the ocean strive to be in equilibrium, and globally the integrated air–sea CO_2 flux equates to 0, though with significant regional fluxes linked to ocean circulation, biology, and solubility (Gruber et al., 2009; Mikaloff-Fletcher et al., 2007).

Considering external sources of carbon to the ocean, however, complicates this picture. Lateral transport of carbon from the land alters the steady state, and the pre-industrial surface ocean becomes supersaturated, highlighting that the pre-industrial ocean was a net source of CO_2 to the atmosphere (Gruber et al., 2009; Mikaloff-Fletcher et al., 2007). The magnitude of this lateral carbon transport is still uncertain and varies between studies, suggesting a flux of 0.21 Pg C/yr (Lacroix et al., 2019), 0.45 Pg C/yr (Jacobson et al., 2007), 0.65 Pg C/yr (Regnier et al., 2022), and 0.78 Pg C/yr (Resplandy et al., 2018).

While the pre-industrial ocean is estimated to be a source of carbon to the atmosphere (Gruber et al., 2009; Mikaloff Fletcher et al., 2007), the present-day ocean is a net carbon sink, taking up ~25% of all human emissions (Friedlingstein et al., 2022). Following the simple notion of the steady-state ocean, the present-day or contemporary air–sea CO_2 flux can simply be viewed as the sum of the pre-industrial state (F_{pre}) and the anthropogenic perturbation (F_{anth}):

$$\mathbf{F}_{\mathrm{cont}} = \mathbf{F}_{\mathrm{anth}} + \mathbf{F}_{\mathrm{pre}} \tag{19}$$

with

$$\mathbf{F}_{\mathrm{pre}} = \mathbf{F}_{\mathrm{nat}} + \mathbf{F}_{\mathrm{riv}} \tag{20}$$

This simplified formulation, however, assumes that circulation, river fluxes, sedimentation, or biological activity has not significantly changed in time. Therefore, a more refined approach considering both steady-state and non-steady-state components of each term in Equations (19)

and (20) is required to understand the contemporary carbon cycle (see, e.g., Hauck et al., 2020). Yet, very little is known about the temporal changes in the river-derived CO_2 and changes in the biological carbon pump (Henson et al., 2016).

Returning to the recent past and the SeaFlux pCO_2 (Fay et al., 2021), based on the surface ocean CO_2 measurement network, one can identify the different timescales of pCO_2 variability. Considering the seasonality of the CO_2 drivers, it appears sensible to first investigate the seasonal marine pCO_2 variations. The map in the center of Figure 5 illustrates the boreal winter (represented by the months of December, January, and February) minus the boreal summer (represented by the months of June, July, and August) partial pressure of CO_2. Indeed, in line with the findings of Takahashi et al. (2002) and Landschützer et al. (2018), the resulting spatial map illustrates two significant features. First, the zonally uniform boundaries at 20° and 40° north and south, and second, the seasonal carbon cycle in the subtropics of both hemispheres is opposing the seasonal cycle of the subpolar regions (Takahashi et al., 2002).

Focusing first on the subtropical ocean (i.e., between 20° and 40° north and south, respectively), the seasonal pCO_2 maximum can be identified in summer (Figure 5), indicating that seasonal temperature variations dominate the variations (Landschützer et al., 2018; Takahashi et al., 2002). In the high latitudes (poleward of 40° north and south, respectively) the opposing seasonal cycle can be observed, highlighting that solubility cannot be the dominating mechanism in these latitudes, and the non-thermal drivers (mixing, biology) dominate the carbon cycle.

Poleward of 40°, however, there are some interesting interhemispheric differences in Figure 5. Particularly in the Indian and Pacific sectors of the Southern Ocean, no strong winter minus summer seasonal cycle can be observed between 40° and 60° S. This may point either toward the inability to reconstruct the seasonality from the limited measurements available, or towards mid-seasonal maxima/minima, linked to spring or autumn biological production. Mongwe et al. (2018) previously highlighted the lack of process knowledge in these regions.

Analyzing the longer-term evolution of the pCO_2 (see the time series in Figure 5), several interesting features emerge. The continuous increase in the atmospheric CO_2 concentration since the industrialization (Dlugokencky & Tans, 2018) has changed the saturation concentration of the surface ocean CO_2 Equation (5). Throughout the ocean, the anthropogenic component (F_{anth}; see Equation (19)) has increased and is responsible for the increase in the contemporary net uptake of CO_2 as opposed to the pre-industrial ocean source of CO_2. As a result, the sea surface pCO_2 follows steadily from 1990 onward (red lines in Figure 5). This change is visible in all latitudes irrespective of the strength and phase of the seasonal cycle and other variations over the past 30 years and is in agreement with local time series station at fixed locations that have observed the sea surface pCO_2 content directly (see, e.g., Bates et al., 2014).

Besides the long-term increase in the sea surface pCO_2, the second dominant signal Figure 5 is the seasonal cycle, with the exception of the tropical band, where little seasonal variation exists. In the subtropical and subpolar band of the northern hemisphere, the seasonal CO_2 minima of the

last 2–3 years have reached values comparable with the seasonal maxima in the early 1990s; whereas in the southern hemisphere, the seasonal CO_2 minima now well exceed the maximum values from the early 1990s.

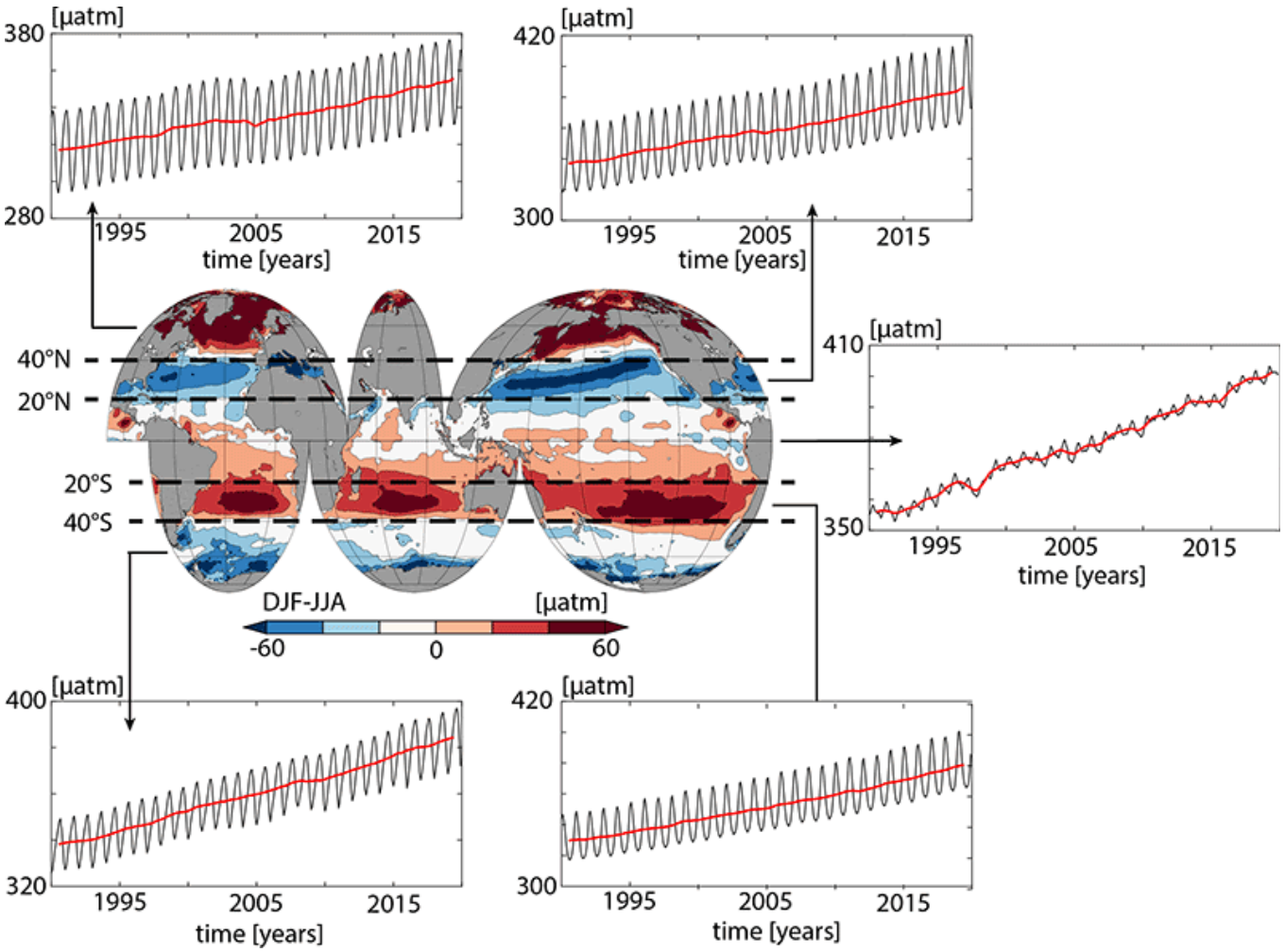

Figure 5. Seasonal through interannual variations in the sea surface pCO_2 from the SeaFlux dataset (Fay et al., 2021). The map in the center illustrates the boreal winter–summer mean amplitude of the seasonal carbon cycle from 1990 to 2019. The time series for the various latitudes show the temporal evolution of the sea surface pCO_2. Black lines illustrate the monthly pCO_2 time series, whereas red lines show the deseasonalized time series.

Source: Author.

Buried under the larger long-term trend and seasonal cycle, shorter-term variations also emerge (Figure 6). De-seasonalizing and detrending the pCO_2 time series reveals several different fluctuations on various timescales (Fay & McKinley, 2013; Landschützer et al., 2019). The tropical band is dominated by the 3- to 7-year variations driven by the El Niño Southern Oscillation variability (Feely et al., 2006). During El Niño periods, reduced upwelling of carbon-rich deep waters lowers the surface pCO_2 significantly, as evident from the strong El Niño year 1998 (see Figure 6), whereas the opposing effect occurs during La Niña periods. Note, though, that due to the average over the full zonal band in the tropics, the drawdown appears weaker as it is

dampened by the Atlantic and Indian Oceans, which do not experience the El Niño Southern Oscillation (ENSO) effect directly (see also Figure 1). Landschützer et al. (2019) have shown that the magnitude of the pCO_2 variability is about three times larger for the tropical Pacific compared to other regions.

In the mid- and higher latitude bands, strong vacillations are visible in the SeaFlux pCO_2, but at much lower frequency. Particularly striking are the sharp pCO_2 decline in the northern hemisphere in 2005 and in the high-latitude Southern Ocean in 2010. These low-frequency variations in the sea surface pCO_2 drive the decadal air–sea CO_2 flux variations, with high-frequency variations dominating in the low latitudes and low-frequency variations dominating in the high latitudes (Landschützer et al., 2016).

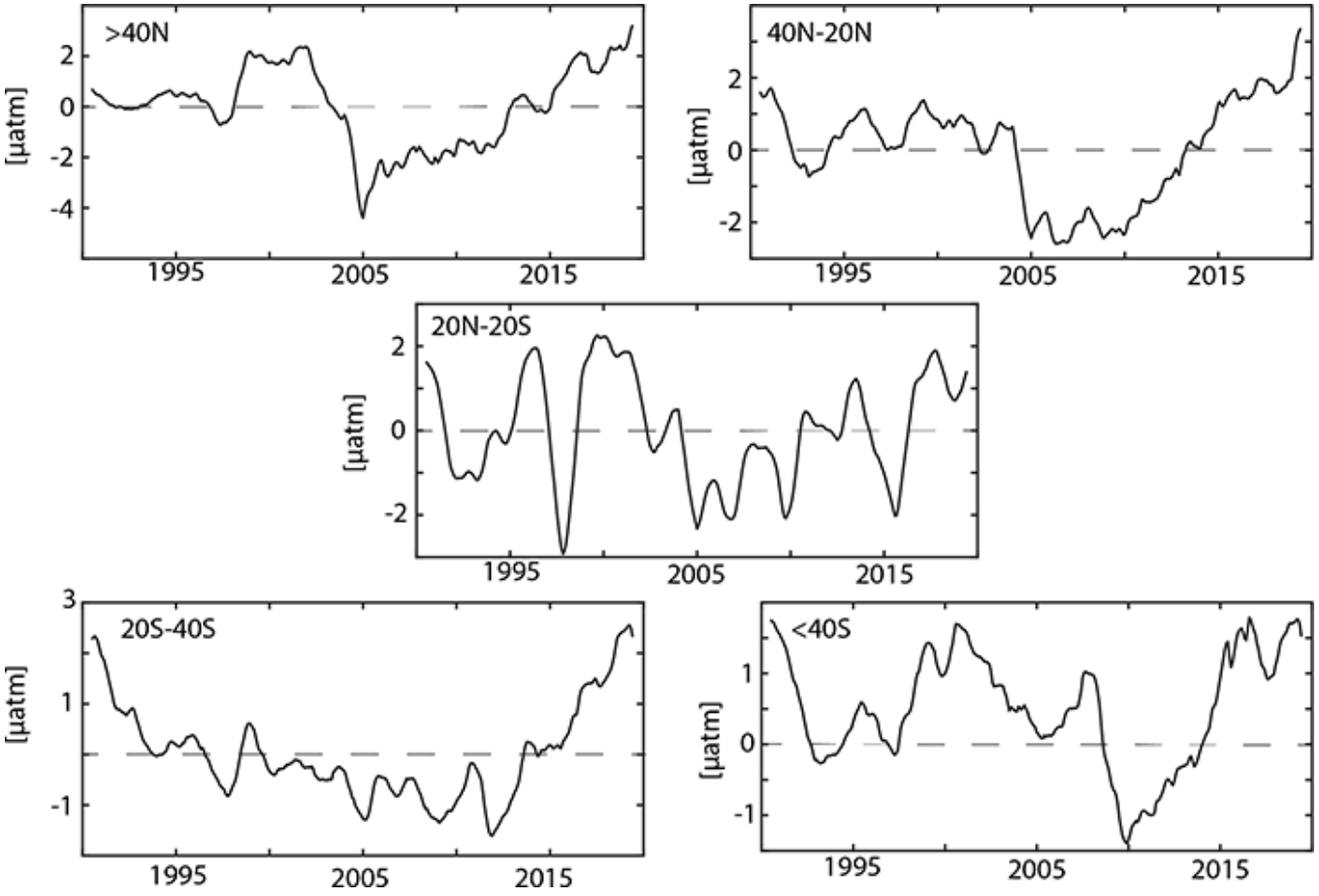

Figure 6. Anomalies (deseasonalized and detrended) in the sea surface pCO_2 over the same latitude bands as in Figure 5. Dashed lines indicate the zero line.

Source: Author.

The origin of these vacillations, in particular of the low frequency in the Southern Ocean, remains largely unresolved, in part as the result of the still rather short observational record. In the early 2000s, primarily model studies suggested that the poleward shift and intensification of the westerly wind belt in the Southern Ocean led to an intensification in the zonal upwelling of deep and carbon-rich ocean waters, resulting in a significant increase in the pCO_2 and outgassing of

carbon from this region, in turn causing an overall saturation of the Southern Ocean carbon sink (Le Quéré et al., 2007). A decade later, first observation-based evidence confirmed this slowdown of the sink, but also reported a bounce-back of the Southern Ocean carbon sink in the late 2000s to its expected strength (DeVries et al., 2017; Keppler & Landschützer, 2019; Landschützer et al., 2015; Munro et al., 2015). The origin of these variations is still debated (DeVries, 2022) and ranges from external forcing linked to volcanic activities (McKinley et al., 2020) through changes in the physical transport linked to weakening/strengthening of the shallow overturning circulation (DeVries et al., 2019), to local changes in the wind-driven circulation (Keppler & Landschützer, 2019) delivering carbon-rich deep waters back to the surface. Given the poor observational coverage in the southern hemisphere (Gloege et al., 2021), also the magnitude of the variations is still debated. Autonomous floats equipped with biogeochemistry sensors may provide the answer. In the recent past, they have already shown that the surface Southern Ocean supply of carbon-rich deep water may be stronger than expected (Gray et al., 2018), questioning the overall sink strength of this basin (Bushinsky et al., 2019).

Impacts of a Changing Carbon Cycle

The increasing concentration of (dissolved) carbon dioxide has manifold consequences for the ocean as an ecosystem and as a habitat for marine life (Doney et al., 2009; Feely et al., 2004, 2009). As shown in the section "CO_2 in the Surface Ocean," a byproduct of the dissolution of excess CO_2 in the ocean is hydrogen ion (H^+). Defined as

$$\mathrm{pH} = -\log\left(\left[\mathrm{H}^{+}\right]\right) \tag{21}$$

the increasing uptake of carbon dioxide by the oceans results in a decline in the sea surface pH through the dissolution and release of hydrogen ion to the seawater—a process in the literature often referred to as ocean acidification (see, e.g., Doney et al., 2009). Since industrialization, the global mean pH declined by about 0.1 (Feely et al., 2009; Jiang et al., 2019) and is visible in all ocean basins from observations (Gregor & Gruber, 2021; Jiang et al., 2019; Lauvset et al., 2015). Current pH is the lowest in the last 24,000 years and is uncommon over the past 2 million years (Gulev et al., 2021).

The additional uptake of CO_2 and its dissolution, therefore, has significant consequences for marine biota producing $CaCO_3$ shells, particularly in regions with low saturation states (Gruber et al., 2012; Orr et al., 2005). The saturation state definition is (Sarmiento & Gruber, 2006):

$$\Omega = \frac{\left[\mathrm{CO}_3^{2-}\right]\left[\mathrm{Ca}^{2+}\right]}{\left[\mathrm{CO}_3^{2-}\right]_{\mathrm{sat}}\left[\mathrm{Ca}^{2+}\right]_{\mathrm{sat}}} \approx \frac{\left[\mathrm{CO}_3^{2-}\right]}{\left[\mathrm{CO}_3^{2-}\right]_{\mathrm{sat}}} \tag{22}$$

Usually, surface waters are supersaturated ($\Omega > 1$) with respect to calcite and aragonite, whereas in the deep ocean, saturation-stated drop ($\Omega < 1$) causing the dissolution of calcium carbonate with depth. Therefore, the abundance of $[CO_3^{2-}]$ is a key factor of the $CaCO_3$ pump. Currently, the ocean is alkaline with an average pH of 8.1 (Fassbender et al., 2021). Looking at the dissolved CO_2 species in Equations (7)–(9), in acidic waters, CO_2 is the most abundant, whereas in alkaline waters, CO_3^{2-} is the most abundant species. In close to neutral conditions, HCO_3^- is the most abundant species. This is well illustrated e.g. in the Bjerrum diagram (see e.g. Sarmiento and Gruber 2006). As the pH of the ocean decreases, free hydrogen ions will form a bond with CO_3^{2-}, reversing Equation (9) (Sarmiento & Gruber, 2006; Zeebe & Wolf-Gladrow, 2001) and lowering the availability for marine biota to form $CaCO_3$ shells. First surface waters to experience such undersaturation conditions have been identified in the high latitudes and the eastern boundary upwelling systems (Gruber et al., 2012).

The expected changes in the carbonate chemistry are not uniform in time, (Hauck & Völker, 2015; Kwiatkowski & Orr, 2018). Observational studies have shown that the seasonal carbon cycle has already amplified (Fassbender et al., 2018; Hauck & Völker, 2015; Landschützer et al., 2018; Rodgers et al., 2008) as a result of both ocean warming and a changing ocean capacity to buffer human-made carbon dioxide (Hauck & Völker, 2015; Landschützer et al., 2018). Therefore, critical saturation states of calcifying minerals are expected to be crossed earlier in time in certain months of the year (Gruber et al., 2012; Kwiatkowski & Orr, 2018), providing a significant stressor for marine ecosystems from primary producers all the way to fisheries.

Conclusions

The increasing number of marine pCO_2 measurements (Bakker et al., 2016) has led to a significant advancement in the estimation of the sea surface pCO_2 and the resulting air–sea CO_2 fluxes, i.e., a critical component of the global carbon budget (Friedlingstein et al., 2022), significantly improving the understanding of regional processes driving the marine carbon cycle. While a decade ago, a climatological mean estimate of the air–sea CO_2 exchange was the state of the art (Takahashi et al., 2009), today, several estimates exist covering multiple decades of sea surface pCO_2 and air–sea CO_2 flux at global scale (Fay et al., 2021). One of the most remarkable findings was the discovery of larger-than-expected variations of the air–sea CO_2 flux (DeVries et al., 2019; Landschützer et al., 2016); however, data sparsity remains still a major challenge, particularly in the data-sparse Southern Ocean (Gloege et al., 2021). Here, newly emerging measurement technologies (Sutton et al., 2021; Williams et al., 2017) started to fill present-day data gaps. Closing the existing data gaps and reducing the uncertainty of the air–sea CO_2 exchange is of prime importance, in light of current and future human greenhouse gas emissions. Furthermore, understanding the evolution of the solubility and biological carbon pumps as well as their relative dominance in controlling the marine carbon cycle will be of prime importance to improve future predictions and projections and to better monitor the dire consequences from ocean acidification for marine life.

Further Reading

Friedlingstein, P., Jones, M. W., O'Sullivan, M., Andrew, R. M., Bakker, D. C. E., Hauck, J., Le Quéré, C., Peters, G. P., Peters, W., Pongratz, J., Sitch, S., Canadell, J. G., Ciais, P., Jackson, R. B., Alin, S. R., Anthoni, P., Bates, N. R., Becker, M., Bellouin, N., . . . Zeng, J. (2022). Global carbon budget 2021 <https://doi.org/10.5194/essd-14-1917-2022>. *Earth System Science Data*, *14*, 1917–2005.

Garbe, C. S., Rutgersson, A., Boutin, J., de Leeuw, G., Delille, B., Fairall, C. W., Gruber, N., Hare, J., Ho, D. T., Johnson, M. T., Nightingale, P. D., Pettersson, H., Piskozub, J., Sahlée, E., Tsai, W.-t., Ward, B., Woolf, D. K., & Zappa, C. J. (2014). Ocean–atmosphere interactions of gases and particles. In P. S. Liss & M. T. Johnson (Eds.), *Transfer across the air-sea interface* (pp. 55–112). Springer.

Gruber, N., Clement, D., Carter, B. R., Feely, R. A., van Heuven, S., Hoppema, M., Ishii, M., Key, R. M., Kozyr, A., Lauvset, S. K., Lo Monaco, C., Mathis, J. T., Murata, A., Olsen, A., Perez, F. F., Sabine, C. L., Tanhua, T., & Wanninkhof, R. (2019). The oceanic sink for anthropogenic CO_2 from 1994 to 2007. *Science*, 363(6432), 1193–1199

Gruber, N., Gloor, M., Mikaloff Fletcher, S. E., Doney, S. C., Dutkiewicz, S., Follows, M. J., Gerber, M., Jacobson, A. R., Joos, F., Lindsay, K., Menemenlis, D., Mouchet, A., Müller, S. A., Sarmiento, J. L., & Takahashi, T. (2009). Oceanic sources, sinks, and transport of atmospheric CO_2 <https://doi.org/10.1029/2008GB003349>. *Global Biogeochemical Cycles*, *23*, GB1005.

Hauck, J., Zeising, M., Le Quéré, C., Gruber, N., Bakker, D. C. E., Bopp, L., Chau, T. T. T., Gürses, O., Ilyina, T., Landschützer, P., Lenton, A., Resplandy, L., Rödenbeck, C., Schwinger, J., & Séférian, R. (2020). Consistency and challenges in the ocean carbon sink estimate for the global carbon budget <https://doi.org/10.3389/fmars.2020.571720>. *Frontiers in Marine Science*, *7*, 571720.

Landschützer, P., Gruber, N., & Bakker, D. C. E. (2016). Decadal variations and trends of the global ocean carbon sink <https://doi.org/10.1002/2015GB005359>. *Global Biogeochemical Cycles*, *30*, 1396–1417.

Millero, F. J. (2013). *Chemical oceanography* (4th ed.). CRC Press.

Regnier, P., Resplandy, L., Najjar, R. G., & Ciais, P. (2022). The land-to-ocean loops of the global carbon cycle <https://doi.org/10.1038/s41586-021-04339-9>. *Nature*, *603*, 401–410.

Sarmiento, J., & Gruber, N. (2006). *Ocean biogeochemical dynamics* (p. 503). Princeton University Press.

Takahashi, T., Sutherland, S. C., Sweeney, C., Poisson, A., Metzl, N., Tilbrook, B., Bates, N., Wanninkhof, R., Feely, R. A., Sabine, C., Olafsson, J., & Nojiri, Y. (2002). Global sea-air CO_2 flux based on climatological surface ocean pCO_2, and seasonal biological and temperature effects. *Deep-Sea Research Part II*, *49*, 1601–1622.

Zeebe, P. E., & Wolf-Gladrow, D. (2001). *CO_2 in seawater: Equilibrium, kinetics, isotopes*. Elsevier.

References

Arruda, R., Atamanchuk, D., Cronin, M., Steinhoff, T., & Wallace, D. W. R. (2020). At-sea intercomparison of three underway pCO_2 systems <https://doi.org/10.1002/lom3.10346>. *Limnology and Oceanography: Methods*, *18*, 63–76.

Bakker, D. C. E., Pfeil, B., Landa, C. S., Metzl, N., O'Brien, K. M., Olsen, A., Smith, K., Cosca, C., Harasawa, S., Jones, S. D., Nakaoka, S., Nojiri, Y., Schuster, U., Steinhoff, T., Sweeney, C., Takahashi, T., Tilbrook, B., Wada, C., Wanninkhof, R., . . .Xu, S. (2016). A multidecade record of high-quality fCO_2 data in version 3 of the Surface Ocean CO_2 Atlas (SOCAT). *Earth System Science Data*, 8, 383–413.

Bakker, D. C. E., Pfeil, B., Smith, K., Hankin, S., Olsen, A., Alin, S. R., Cosca, C., Harasawa, S., Kozyr, A., Nojiri, Y., O'Brien, K. M., Schuster, U., Telszewski, M., Tilbrook, B., Wada, C., Akl, J., Barbero, L., Bates, N. R., Boutin, J., . . . Watson, A. J. (2014). An update to the Surface Ocean CO_2 Atlas (SOCAT version 2) <https://doi.org/10.5194/essd-6-69-2014>. *Earth System Science Data*, *6*(1), 69–90.

Bates, N. R., Astor, Y. M., Church, M. J., Currie, K., Dore, J. E., González-Dávila, M., Lorenzoni, L., Muller-Karger, F., Olafsson, J., & Santana-Casiano, J. M. (2014). A time-series view of changing ocean chemistry due to ocean uptake of anthropogenic CO_2 and ocean acidification. *Oceanography*, *27*, 126–141.

Bushinsky, S. M., Landschützer, P., Rödenbeck, C., Gray, A. R., Baker, D., Mazloff, M. R., Resplandy, L., Johnson, K. S., & Sarmiento, J. L. (2019). Reassessing Southern Ocean air–sea CO_2 flux estimates with the addition of biogeochemical float observations <https://doi.org/10.1029/2019GB006176>. *Global Biogeochemical Cycles*, *33*, 1370–1388.

Chau, T. T. T., Gehlen, M., & Chevallier, F. (2020). *Quality information document for Global Ocean Surface Carbon Product MULTIOBS_ GLO_BIO_CARBON_SURFACE_REP_015_008* <https://hal.archives-ouvertes.fr/hal-02957656/file/CMEMS-MOB-QUID-015-008.pdf> [PhD dissertation, Le Laboratoire des Sciences du Climat et de l'Environnement].

Cooper, D. J., Watson, A. J., & Ling, R. D. (1998). Variation of PCO_2 along a North Atlantic shipping route (U.K. to the Caribbean): A year of automated observations. *Marine Chemistry*, *60*, 147–164.

Dai, M., Su, J., Zhao, Y., Hofmann, E. E., Cao, Z., Cai, W. J., Gan, J., Lacroix, F., Laruelle, G. G., Meng, F., Müller, J. D., Regnier, P. A. G., Wang, G., & Wang, Z. (2022). Carbon fluxes in the coastal ocean: Synthesis, boundary processes and future trends. *Annual Review of Earth and Planetary Sciences*, *50*(1), 593–626.

Deacon, E. L. (1977). Gas transfer to and across an air-water interface. *Tellus*, *29*, 363–374.

Denvil-Sommer, A., Gehlen, M., Vrac, M., & Mejia, C. (2019). LSCEFFNN- v1: A two-step neural network model for the reconstruction of surface ocean pCO_2 over the global ocean <https://doi.org/10.5194/gmd-12-2091-2019>. *Geoscientific Model Development*, *12*, 2091–2105.

DeVries, T. (2022). Atmospheric CO_2 and sea surface temperature variability cannot explain recent decadal variability of the ocean CO_2 sink. *Geophysical Research Letters*, *49*, 1–12.

DeVries, T., Holzer, M., & Primeau, F. (2017). Recent increase in oceanic carbon uptake driven by weaker upper-ocean overturning <https://doi.org/10.1038/nature21068>. *Nature*, *542*, 215–218.

DeVries, T., Le Quéré, C., Andrews, O., Berthet, S., Hauck, J., Ilyina, T., Landschützer, P., Lenton, A., Lima, I. D., Nowicki, M., Schwinger, J., & Séférian, R. (2019). Decadal trends in the ocean carbon sink <https://doi.org/10.1073/pnas.1900371116>. *Proceedings of the National Academy of Sciences*, *116*(24), 11646–11651.

Dickson, A. G., & Goyet, C. (1994). *Handbook of methods for the analysis of various parameters of the carbon dioxide system in seawater*, ORNL/CDIAC-74. Oak Ridge National Laboratory.

Dickson, A. G., Sabine, C. L., & Christian, J. R., (Eds.). (2007). *Guide to best practices for ocean CO_2 measurements*, IOCCP Report No. 8. PICES Special Publication.

Dlugokencky, E., & Tans, P. (2018). *Trends in atmospheric carbon dioxide <http://www.esrl.noaa.gov/gmd/ccgg/trends/global.html>*. National Oceanic & Atmospheric Administration, Earth System Research Laboratory.

Doney, S. C., Fabry, V. J., Feely, R. A., & Kleypas, J. A. (2009). Ocean acidification: The other CO_2 problem. *Annual Review of Marine Science*, *1*, 169–192.

Fassbender, A. J., Orr, J. C., & Dickson, A. G. (2021). Technical note: Interpreting pH changes *<https://doi.org/10.5194/bg-18-1407-2021>*. *Biogeosciences*, *18*, 1407–1415.

Fassbender, A. J., Rodgers, K. B., Palevsky, H. I., & Sabine, C. L. (2018). Seasonal asymmetry in the evolution of surface ocean pCO_2 and pH thermodynamic drivers and the influence on sea-air CO_2 flux *<https://doi.org/10.1029/2017GB005855>*. *Global Biogeochemical Cycles*, *32*, 1476–1497.

Fay, A. R., Gregor, L., Landschützer, P., McKinley, G. A., Gruber, N., Gehlen, M., Iida, Y., Laruelle, G. G., Rödenbeck, C., Roobaert, A., & Zeng, J. (2021). Harmonization of global surface ocean Pco_2 mapped products and their flux calculations: An improved estimate of the ocean carbon sink *<https://doi.org/10.5194/essd-13-4693-2021>*. *Earth System Science Data*, *13*, 4693–4710.

Fay, A. R., & McKinley, G. A. (2013). Global trends in surface ocean pCO_2 from in situ data *<https://doi.org/10.1002/gbc.20051>*. *Global Biogeochemical Cycles*, *27*, 541–557.

Feely, R. A., Doney, S. C., & Cooley, S. R. (2009). Ocean acidification: Present conditions and future changes in a high-CO_2 world *<https://doi.org/10.5670/oceanog.2009.95>*. *Oceanography*, *22*(4), 36–47.

Feely, R. A., Sabine, C. L., Lee, K., Berelson, W., Kleypas, J., Fabry, V. J., & Millero, F. J. (2004). Impact of anthropogenic CO_2 on the $CaCO_3$ system in the oceans *<https://www.science.org/doi/10.1126/science.1097329>*. *Science*, *305* (5682), 362–366.

Feely, R. A., Takahashi, T., Wanninkhof, R., McPhaden, M. J., Cosca, C. E., Sutherland, S. C., & Carr, M.-E. (2006). Decadal variability of the air–sea CO_2 fluxes in the equatorial Pacific Ocean *<https://doi.org/10.1029/2005JC003129>*. *Journal of Geophysical Research*, *111*, C08S90.

Franco, A. C., Gruber, N., Frölicher, T. L., & Kropuenske Artman, L. (2018). Contrasting impact of future CO_2 emission scenarios on the extent of $CaCO_3$ mineral undersaturation in the Humboldt current system *<https://doi.org/10.1002/2018JC013857>*. *Journal of Geophysical Research Oceans*, *123*, 2018–2036.

Friedlingstein, P., Jones, M. W., O'Sullivan, M., Andrew, R. M., Bakker, D. C. E., Hauck, J., Le Quéré, C., Peters, G. P., Peters, W., Pongratz, J., Sitch, S., Canadell, J. G., Ciais, P., Jackson, R. B., Alin, S. R., Anthoni, P., Bates, N. R., Becker, M., Bellouin, N., . . . Zeng, J. (2022). Global carbon budget 2021 *<https://doi.org/10.5194/essd-14-1917-2022>*. *Earth System Science Data*, *14*, 1917–2005.

Frölicher, T. L., Sarmiento, J. L., Paynter, D. J., Dunne, J. P., Krasting, J. P., & Winton, M. (2015). Dominance of the Southern Ocean in anthropogenic carbon and heat uptake in CMIP5 models. *Journal of Climate*, *28*, 862–886.

Garbe, C. S., Rutgersson, A., Boutin, J., de Leeuw, G., Delille, B., Fairall, C. W., Gruber, N., Hare, J., Ho, D. T., Johnson, M. T., Nightingale, P. D., Pettersson, H., Piskozub, J., Sahlée, E., Tsai, W-t., Ward, B., Woolf, D. K., & Zappa, C. J. (2014). Transfer across the air-sea interface. In *Ocean-atmosphere interactions of gases and particles* (pp. 55–112). Springer.

Gloege, L., McKinley, G. A., Landschützer, P., Fay, A. R., Frölicher, T. L., Fyfe, J. C., Ilyina, T., Jones, S., Lovenduski, N. S., Rodgers, K. B., Schlunegger, S., & Takano, Y. (2021). Quantifying errors in observationally-based estimates of ocean carbon sink variability. *Global Biogeochemical Cycles*, *35*, e2020GB006788.

Gray, A. R., Johnson, K. S., Bushinsky, S. M., Riser, S. C., Russell, J. L., Talley, L. D., Wanninkhof, R., Williams, N. L., & Sarmiento, J. L. (2018). Autonomous biogeochemical floats detect significant carbon dioxide outgassing in the high-latitude Southern Ocean. *Geophysical Research Letters*, *45*, 9049– 9057

Gregor, L., & Gruber, N. (2021). OceanSODA-ETHZ: A global gridded data set of the surface ocean carbonate system for seasonal to decadal studies of ocean acidification. *Earth System Science Data*, 13, 777–808.

Gregor, L., Lebehot, A. D., Kok, S., & Scheel Monteiro, P. M. (2019). A comparative assessment of the uncertainties of global surface ocean CO_2 estimates using a machine-learning ensemble (CSIR-ML6 version 2019a): Have we hit the wall? *<https://doi.org/10.5194/gmd-12-5113-2019> Geoscientific Model Development*, *12*, 5113–5136.

Gruber, N. (2019). The oceanic sink for anthropogenic CO_2 from 1994 to 2007. *Science*, 363(6432), 1193–1199.

Gruber, N., Gloor, M., Mikaloff Fletcher, S. E., Doney, S. C., Dutkiewicz, S., Follows, M. J., Gerber, M., Jacobson, A. R., Joos, F., Lindsay, K., Menemenlis, D., Mouchet, A., Müller, S. A., Sarmiento, J. L., & Takahashi, T. (2009). Oceanic sources, sinks, and transport of atmospheric CO_2 *<https://doi.org/10.1029/2008GB003349>*. *Global Biogeochemical Cycles*, *23*, GB1005.

Gruber, N., Hauri, C., Lachkar, Z., Loher, D., Frölicher, T. L., & Plattner, G. K. (2012). Rapid progression of ocean acidification in the California current system. *Science*, *337*, 220–223.

Gruber, N., Landschützer, P., & Lovenduski, N. S. (2019). The variable Southern Ocean carbon sink *<https://doi.org/10.1146/annurev-marine-121916-063407>*. *Annual Review of Marine Science*, *11*(1), 159–186.

Gulev, S. K., Thorne, P. W., Ahn, J., Dentener, F. J., Domingues, C. M., Gerland, S., Gong, D., Kaufman, D. S., Nnamchi, H.C., Quaas, J., Rivera, J.A., Sathyendranath, S., Smith, S.L., Trewin, B., von Schuckmann, K., & Vose, R. S. (2021). *Changing state of the climate system* *<https://www.10.1017/9781009157896.004,%202021>*. Climate Change 2021: The Physical Science Basis. Contribution of Working Group I to the Sixth Assessment Report of the Intergovernmental Panel on Climate Change (V. Masson-Delmotte, P. Zhai, A. Pirani, S. L. Connors, C. Péan, S. Berger, N. Caud, Y. Chen, L. Goldfarb, M. I. Gomis, M. Huang, K. Leitzell, E. Lonnoy, J. B. R. Matthews, T. K. Maycock, T. Waterfield, O. Yelekçi, R. Yu, & B. Zhou, Eds., pp. 287–422). Cambridge University Press.

Hauck, J., & Völker, C. (2015). Rising atmospheric CO_2 leads to large impact of biology on Southern Ocean CO_2 uptake via changes of the Revelle factor. *Geophysical Research Letters*, 42, 1459–1464.

Hauck, J., Zeising, M., Le Quéré, C., Gruber, N., Bakker, D. C. E., Bopp, L., Chau, T. T. T., Gürses, Ö., Ilyina, T., Landschützer, P., Lenton, A., Resplandy, L., Rödenbeck, C., Schwinger, J., & Séférian, R. (2020). Consistency and challenges in the ocean carbon sink estimate for the global carbon budget *<https://doi.org/10.3389/fmars.2020.571720>*. *Frontiers in Marine Science*, *7*, 571720.

Heinze, C., Meyer, S., Goris, N., Anderson, L., Steinfeldt, R., Chang, N., Le Quéré, C., & Bakker, D. C. E. (2015). The ocean carbon sink: Impacts, vulnerabilities and challenges <https://doi.org/10.5194/esd-6-327-2015>. *Earth System Dynamics*, *6*, 327–358.

Henson, S. A., Beaulieu, C., & Lampitt, R. (2016). Observing climate change trends in ocean biogeochemistry: When and where <https://doi.org/10.1111/gcb.13152>. *Global Change Biology*, *22*, 1561–1571.

Henson, S. A., Sanders, R., Madsen, E., Morris, P. J., Le Moigne, F., & Quartly, G. D. (2011). A reduced estimate of the strength of the ocean's biological carbon pump <https://doi.org/10.1029/2011GL046735>. *Geophysical Research Letters*, *38*, L04606.

Humphreys, M. P., Lewis, E. R., Sharp, J. D., & Pierrot, D. (2022). PyCO$_2$SYS v1.8: Marine carbonate system calculations in python <https://doi.org/10.5194/gmd-15-15-2022>. *Geoscientific Model Development*, *15*, 15–43.

Iida, Y., Takatani, Y., Kojima, A., & Ishii, M. (2020). Global trends of ocean CO_2 sink and ocean acidification: An observation based reconstruction of surface ocean inorganic carbon variables <https://doi.org/10.1007/s10872-020-00571-5>. *Journal of Oceanography*, *77*, 323–358.

Jacobson, A. R., Mikaloff Fletcher, S. E., Gruber, N., Sarmiento, J. L., & Gloor, M. (2007). A joint atmosphere-ocean inversion for surface fluxes of carbon dioxide-2: Regional results <https://doi.org/10.1029/2006GB002703>. *Global Biogeochemical Cycles*, *21*, GB1020.

Jähne, B., Münnich, K. O., Bösinger, R., Dutzi, A., Huber, W., & Libner, P. (1987). On parameters influencing air-water gas exchange. *Journal of Geophysical Research*, *92*, 1937–1949.

Jiang, L-Q., Carter, B. R., Feely, R. A., Lauvset, S. K., & Olsen, A. (2019). Surface ocean pH and buffer capacity: Past, present and future <https://doi.org/10.1038/s41598-019-55039-4>. *Scientific Reports*, *9*, 18624.

Jones, S. D., Le Quéré, C., & Rödenbeck, C. (2012). Autocorrelation characteristics of surface ocean pCO_2 and air-sea CO_2 fluxes <https://doi.org/10.1029/2010GB004017>. *Global Biogeochemical Cycles*, *26*, GB2042.

Kalnay, E., Kanamitsu, M., Kistler, R., Collins, W., Deaven, D., Gandin, L., Iredell, M., Saha, S., White, G., Woollen, J., Zhu, Y., Chelliah, M., Ebisuzaki, W., Higgins, W., Janowiak, J., Mo, K. C., Ropelewski, C., Wang, J., Leetmaa, A., . . Joseph, D. (1996). The NCEP/NCAR 40-year reanalysis project. *Bulletin of the American Meteorological Society*, *77*, 437–470.

Keppler, L., & Landschützer, P. (2019). Regional wind variability modulates the Southern Ocean carbon sink <https://doi.org/10.1038/s41598-019-43826-y>. *Scientific Reports*, *9*(1), 1–10.

Keppler, L., Landschützer, P., Gruber, N., Lauvset, S. K., & Stemmler, I. (2020). Seasonal carbon dynamics in the near-global ocean <https://doi.org/10.1029/2020GB006571>. *Global Biogeochemical Cycles*, *34*, e2020GB006571.

Khatiwala, S., Tanhua, T., Mikaloff Fletcher, S., Gerber, M., Doney, S. C., Graven, H. D., Gruber, N., McKinley, G. A., Murata, A., Ríos, A. F., & Sabine, C. L. (2013). Global ocean storage of anthropogenic carbon <https://doi.org/10.5194/bg-10-2169-2013>. *Biogeosciences*, *10*, 2169–2191.

Körtzinger, A., Thomas, H., Schneider, B., Gronau, N., Mintrop, L., & Duinker, J. C. (1996). At-sea intercomparison of two newly designed underway pCO_2 systems–Encouraging results. *Marine Chemistry*, *52*, 122–145.

Kwiatkowski, L., & Orr, J. (2018). Diverging seasonal extremes for ocean acidification during the twenty-first century. *Nature Climate Change*, *8*, 141–145.

Lacroix, F., Ilyina, T., & Hartmann, J. (2019). Oceanic CO_2 outgassing and biological production hotspots induced by pre-industrial river loads of nutrients and carbon in a global modelling approach <https://doi.org/10.5194/bg-2019-152>. *Biogeosciences Discussions*.

Landschützer, P., Gruber, N., & Bakker, D. C. E. (2016). Decadal variations and trends of the global ocean carbon sink. *Global Biogeochemical Cycles*, 30, 1396–1417.

Landschützer, P., Gruber, N., Bakker, D. C. E., & Schuster, U. (2014). Recent variability of the global ocean carbon sink <https://doi.org/10.1002/2014GB004853>. *Global Biogeochemical Cycles*, *28*, 927–949.

Landschützer, P., Gruber, N., Bakker, D. C. E., Schuster, U., Nakaoka, S., Payne, M. R., Sasse, T. P., & Zeng, J. (2013). A neural network-based estimate of the seasonal to inter-annual variability of the Atlantic Ocean carbon sink <https://doi.org/10.5194/bg-10-7793-2013>. *Biogeosciences*, *10*, 7793–7815.

Landschützer, P., Gruber, N., Bakker, D. C. E., Stemmler, I., & Six, K. D. (2018). Strengthening seasonal marine CO_2 variations due to increasing atmospheric CO_2. *Nature Climate Change*, 8, 146–150.

Landschützer, P., Gruber, N., Haumann, F. A., Rödenbeck, C., Bakker, D. C. E., van Heuven, S., Hoppema, M., Metzl, N., Sweeney, C., Takahashi, T., Tilbrook, B., & Wanninkhof, R. (2015). The reinvigoration of the Southern Ocean carbon sink <https://doi.org/10.1126/science.aab2620>. *Science*, *349*, 1221–1224.

Landschützer, P., Ilyina, T., & Lovenduski, N. S. (2019). Detecting regional modes of variability in observation-based surface ocean pCO_2. *Geophysical Research Letters*, *46*, 2670–2679.

Landschützer, P., Laruelle, G. G., Roobaert, A., & Regnier, P. (2020). A uniform pCO_2 climatology combining open and coastal oceans <https://doi.org/10.5194/essd-12-2537-2020>. *Earth System Science Data*, *12*, 2537–2553.

Laruelle, G. G., Landschützer, P., Gruber, N., Tison, J.-L., Delille, B., & Regnier, P. (2017). Global high-resolution monthly pCO_2 climatology for the coastal ocean derived from neural network interpolation <https://doi.org/10.5194/bg-14-4545-2017>. *Biogeosciences*, *14*, 4545–4561.

Lauvset, S. K., Gruber, N., Landschützer, P., Olsen, A., & Tjiputra, J. (2015). Trends and drivers in global surface ocean pH over the past 3 decades. *Biogeosciences*, *12*, 1285–1298.

Le Moigne F. A. C. (2019). Pathways of organic carbon downward transport by the oceanic biological carbon pump <https://doi.org/10.3389/fmars.2019.00634>. *Frontiers in Marine Science*, *6*, 634.

Le Quéré, C., Rödenbeck, C., Buitenhuis, E. T., Conway, T. J., Langenfelds, R., Gomez, A., Labuschagne, C., Ramonet, M., Nakazawa, T., Metzl, N., Gillett, N., & Heimann, M. (2007). Saturation of the Southern Ocean CO_2 sink due to recent climate change. *Science*, *316*, 1735–1738.

Lewis, E., & Wallace, D. W. R. (1998). *Program developed for CO_2 system calculations*, ORNL/CDIAC-105. U.S. Department of Energy.

Liss, P. S., & Merlivat, L. (1986). Air-sea gas exchange rates: Introduction and synthesis. In *The role of air-sea exchange in geochemical cycling* (pp. 113–127). D. Reidel.

Liss, P. S., & Slater, P. G. (1974). Flux of gases across the air-sea interface. *Nature*, *247*, 181–184.

Lovecchio, E., Gruber, N., & Münnich, M. (2018). Mesoscale contribution to the long-range offshore transport of organic carbon from the canary upwelling system to the open North Atlantic <https://doi.org/10.5194/bg-15-5061-2018>. *Biogeosciences*, *15*, 5061–5091.

Manning, A. C., & Keeling, R. F. (2006). Global oceanic and land biotic carbon sinks from the Scripps atmospheric oxygen flask sampling network <https://doi.org/10.1111/j.1600-0889.2006.00175.x>. *Tellus B*, *58*, 95–116.

Maritorena, S., Fanton d'Andon, O. H., Mangin, A., & Siegel, D. A. (2010). Merged satellite ocean color data products using a bio-optical model: Characteristics, benefits and issues. *Remote Sensing of Environment*, *114*, 1791–1804.

Marshall, J., & Speer, K. (2012). Closure of the meridional overturning circulation through Southern Ocean upwelling <https://doi.org/10.1038/ngeo1391>. *Nature Geoscience*, *5*, 171–180.

McKinley, G. A., Fay, A. R., Eddebbar, Y. A., Gloege, L., & Lovenduski, N. S. (2020). External forcing explains recent decadal variability of the ocean carbon sink <https://doi.org/10.1029/2019AV000149>. *AGU Advances*, *1*, e2019AV000149.

Mcneil, B. I., Matear, R. J., Key, R. M., Bullister, J. L., & Sarmiento, J. L. (2003). Anthropogenic CO_2 uptake by the ocean based on the global chlorofluorocarbon data set <https://doi.org/10.1126/science.1077429>. *Science*, *299*, 235–239.

Mikaloff Fletcher, S. E., Gruber, N. P., Jacobson, A.R., Doney, S. C., Dutkiewicz, S., Gerber, M., Follows, M., Joos, F., Lindsay, K., Menemenlis, D., Mouchet, A., Muller, S. A., & Sarmiento, J. (2007). Inverse estimates of the oceanic sources and sinks of natural CO_2 and the implied oceanic carbon transport. *Global Biogeochemical Cycles*, *21*, GB1010.

Millero, F. J. (2013). *Chemical oceanography* (4th ed.). CRC Press.

Mongwe, N. P., Vichi, M., & Monteiro, P. M. S. (2018). The seasonal cycle of pCO_2 and CO_2 fluxes in the Southern Ocean: Diagnosing anomalies in CMIP5 Earth system models <https://doi.org/10.5194/bg-15-2851-2018>. *Biogeosciences*, *15*, 2851–2872.

Munro, D. R., Lovenduski, N. S., Takahashi, T., Stephens, B. B., Newberger, T., & Sweeney, C. (2015). Recent evidence for a strengthening CO_2 sink in the Southern Ocean from carbonate system measurements in the Drake Passage (2002–2015) <https://doi.org/10.1002/2015GL065194>. *Geophysical Research Letters*, *42*, 7623–7630.

Olsen, A., Lange, N., Key, R. M., Tanhua, T., Álvarez, M., Becker, S., Bittig, H. C., Carter, B. R., Cotrim da Cunha, L., Feely, R. A., van Heuven, S., Hoppema, M., Ishii, M., Jeansson, E., Jones, S. D., Jutterström, S., Karlsen, M. K., Kozyr, A., Lauvset, S. K., . . . Wanninkhof, R. (2019). GLODAPv2.2019: An update of GLODAPv2 <https://doi.org/10.5194/essd-11-1437-2019>. *Earth System Science Data*, *11*(3), 1437–1461.

Orr, J. C., Fabry, V. J., Aumont, O., Bopp, L., Doney, S. C., Feely, R. A., Gnanadesikan, A., Gruber, N., Ishida, A., Joos, F., Key, R. M., Lindsay, K., Maier-Reimer, E., Matear, R., Monfray, P., Mouchet, A., Najjar, R. G., Plattner, G. K., Rodgers, K. B., . . . Yool, A. (2005). Anthropogenic ocean acidification over the twenty-first century and its impact on calcifying organisms. *Nature*, *437*, 681–686.

Pfeil, B., Olsen, A., Bakker, D. C. E., Hankin, S., Koyuk, H., Kozyr, A., Malczyk, J., Manke, A., Metzl, N., Sabine, C. L., Akl, J., Alin, S. R., Bates, N., Bellerby, R. G. J., Borges, A., Boutin, J., Brown, P. J., Cai, W.-J., Chavez, F. P., . . . Yoshikawa-Inoue,

H. (2013). A uniform, quality-controlled Surface Ocean CO_2 Atlas (SOCAT) <https://doi.org/10.5194/essd-5-125-2013>. *Earth System Science Data*, *5*, 125–143.

Pierrot, D., Neill, C., Sullivan, K., Castle, R., Wanninkhof, R., Lüger, H., Johannessen, T., Olsen, A., Feely, R. A., & Cosca, C. E. (2009). Recommendations for autonomous underway pCO_2 measuring systems and data-reduction routines. *Deep Sea Research Part II: Topical Studies in Oceanography*, *56*(8–10), 512–522

Regnier, P., Friedlingstein, P., Ciais, P., Mackenzie, F. T., Gruber, N., Janssens, I. A., Laruelle, G. G., Lauerwald, R., Luyssaert, S., Andersson, A. J., Arndt, S., Arnosti, C., Borges, A. V., Dale, A. W., Gallego-Sala, A., Goddéris, Y., Goossens, N., Hartmann, J., Heinze, C., . . . Thullner, M. (2013). Anthropogenic perturbation of the carbon fluxes from land to ocean <https://doi.org/10.1038/ngeo1830>. *Nature Geoscience*, *6*, 597–607.

Regnier, P., Resplandy, L., Najjar, R. G., & Ciais, P. (2022). The land-to-ocean loops of the global carbon cycle <https://doi.org/10.1038/s41586-021-04339-9>. *Nature*, *603*, 401–410.

Resplandy, L., Keeling, R. F., Rödenbeck, C., Stephens, B. B., Khatiwala, S., Rodgers, K. B., Long, M. C., Bopp, L., & Tans, P. P. (2018). Revision of global carbon fluxes based on a reassessment of oceanic and riverine carbon transport <https://doi.org/10.1038/s41561-018-0151-3>. *Nature Geoscience*, *11*, 504–509.

Reynolds, R. W., Rayner, N. A., Smith, T. M., Stokes, D. C., & Wang, W. (2002). An improved in situ and satellite SST analysis for climate. *Journal of Climate*, *15*, 1609–1625.

Ritter, R., Landschützer, P., Gruber, N., Fay, A. R., Iida, Y., Jones, S., Nakaoka, S., Park, G.-H., Peylin, P., Rödenbeck, C., Rodgers, K. B., Shutler, J. D., & Zeng, J. (2017). Observation-based trends of the Southern Ocean carbon sink <https://doi.org/10.1002/2017GL074837>. *Geophysical Research Letters*, *44*, 12339–12348.

Rödenbeck, C., Bakker, D. C. E., Gruber, N., Iida, Y., Jacobson, A. R., Jones, S., Landschützer, P., Metzl, N., Nakaoka, S., Olsen, A., Park, G.-H., Peylin, P., Rodgers, K. B., Sasse, T. P., Schuster, U., Shutler, J. D., Valsala, V., Wanninkhof, R., & Zeng, J. (2015). Data-based estimates of the ocean carbon sink variability: The surface ocean pCO_2 mapping intercomparison (SOCOM). *Biogeosciences*, 12, 7251–7278.

Rödenbeck, C., Houweling, S., Gloor, M., & Heimann, M. (2003). CO_2 flux history 1982–2001 inferred from atmospheric data using a global inversion of atmospheric transport Atmos. *Chemical Physics*, *3*, 1919–1964.

Rödenbeck, C., Houweling, S., Gloor, M., & Heimann, M. (2013). Global surface-ocean pCO_2 and sea–air CO_2 flux variability from an observation driven ocean mixed-layer scheme <https://doi.org/10.5194/os-9-193-2013>. *Ocean Science*, *9*, 193–216.

Rodgers, K. B., Sarmiento, J. L., Aumont, O., Crevoisier, C., de Boyer Montégut, C., & Metzl, N. (2008). A wintertime uptake window for anthropogenic CO_2 in the North Pacific. *Global Biochemical Cycles*, *22*, GB2020.

Roobaert, A., Laruelle, G. G., Landschützer, P., & Regnier, P. (2018). Uncertainty in the global oceanic CO_2 uptake induced by wind forcing: Quantification and spatial analysis <https://doi.org/10.5194/bg-15-1701-2018>. *Biogeosciences*, *15*, 1701–1720.

Sabine, C. L., Feely, R. A., Gruber, N., Key, R. M., Lee, K., Bullister, J. L., Wanninkhof, R., Wong, C. S., Wallace, D. W. R., Tilbrook, B., Millero, F. J., Peng, T. H., Kozyr, A., Ono, T., & Rios, A. F. (2004). The oceanic sink for anthropogenic CO_2 <https://doi.org/10.1126/science.1097403>. *Science*, *305*(5682), 367–371.

Sarmiento, J., & Gruber, N. (2006). *Ocean biogeochemical dynamics* (p. 503). Princeton University Press.

Sutton, A. J., Williams, N. L., & Tilbrook, B. (2021). Constraining Southern Ocean CO_2 flux uncertainty using uncrewed surface vehicle observations <https://doi.org/10.1029/2020GL091748>. *Geophysical Research Letters*, *48*, e2020GL091748.

Sweeney, C., Gloor, E., Jacobson, A. R., Key, R. M., McKinley, G., Sarmiento, J. L., & Wanninkhof, R. (2007). Constraining global air-sea gas exchange for CO_2 with recent bomb 14C measurements. *Global Biochemical Cycles*, *21*, GB2015.

Takahashi, T., Olafson, J., Goddard, J., Chipman, D., & Sutherland, S. (1993). Seasonal variations of CO_2 and nutrients in the high-latitudesurface oceans: A comparative study. *Global Biogeochemical Cycles*, 7(4), 843–878.

Takahashi, T., Sutherland, S. C., Sweeney, C., Poisson, A., Metzl, N., Tilbrook, B., Bates, N., Wanninkhof, R., Feely, R. A., Sabine, C., Olafsson, J., & Nojiri, Y. (2002). Global sea-air CO_2 flux based on climatological surface ocean pCO_2, and seasonal biological and temperature effects. *Deep-Sea Research Part II*, *49*, 1601–1622.

Takahashi, T., Sutherland, S. C., & Kozyr, A. (2019). Global Ocean surface water partial pressure of CO_2 database: Measurements performed during 1957–2019 (LDEO database version 2019) (NCEI accession 0160492). Version 9.9. NOAA National Centers for Environmental Information Dataset.

Takahashi, T., Sutherland, S. C., Wanninkhof, R., Sweeney, C., Feely, R. A., Chipman, D. W., Hales, B., Friederich, G., Chavez, F., Sabine, C., Watson, A., Bakker, D. C. E., Schuster, U., Metzl, N., Yoshikawa-Inoue, H., Ishii, M., Midorikawa, T., Nojiri, Y., Körtzinger, A., . . . de Baar, H. J. W. (2009). Climatological mean and decadal change in surface ocean pCO_2, and net sea air CO_2 flux over the global oceans. *Deep-Sea Research Part II*, *56*, 554–577.

Talley, L. D. (2011). *Descriptive physical oceanography* (6th ed.). Elsevier.

van Heuven, S., Pierrot, D., Rae, J. W. B., Lewis, E., & Wallace, D. W. R. (2011). *Matlab program developed for CO_2 system calculations*. ORNL/CDIAC-105b. U.S. Department of Energy.

Wanninkhof, R. (1992). Relation between wind speed and gas exchange over the ocean. *Journal of Geophysical Research*, *97*, 7373–7383.

Wanninkhof, R., & McGillis, W. (1999). A cubic relationship between air-sea CO_2 exchange and wind speed. *Geophysical Research Letters*, *26*(13), 1889–1892.

Watson, A. J., Schuster, U., Shutler, J. D., Holding, T., Ashton, I. G. C., Landschützer, P., Woolf, D. K., & Goddijn-Murphy, L. (2020). Revised estimates of ocean-atmosphere CO_2 flux are consistent with ocean carbon inventory <https://doi.org/10.1038/s41467-020-18203-3>. *Nature Communications*, *11*, 4422.

Weiss, R. F. (1974). Carbon dioxide in water and seawater: The solubility of a non-ideal gas. *Marine Chemistry*, *2*, 203–215.

Williams, N. L., Juranek, L. W., Feely, R. A., Johnson, K. S., Sarmiento, J. L., Talley, L. D., Dickson, A. G., Gray, A. R., Wanninkhof, R., Russell, J. L., Riser, S. C., & Takeshita, Y. (2017). Calculating surface ocean pCO_2 from biogeochemical Argo floats equipped with pH: An uncertainty analysis. *Global Biogeochemical Cycles*, *31*, 591–604.

Woolf, D. K., Land, P. E., Shutler, J. D., Goddijn-Murphy, L. M., & Donlon, C. J. (2016). On the calculation of air-sea fluxes of CO_2 in the presence of temperature and salinity gradients. *Journal of Geophysical Research, Oceans*, *121*, 1229–1248.

Xue, L., Gao, L., Cai, W.-J., Yu, W., & Wei, M. (2015). Response of sea surface fugacity of CO_2 to the SAM shift south of Tasmania: Regional differences. *Geophysical Research Letters*, *42*, 3973–3979.

Zeebe, P. E., & Wolf-Gladrow, D. (2001). *CO_2 in seawater: Equilibrium, kinetics, isotopes*. Elsevier.

Zeng, J., Nojiri, Y., Landschützer, P., Telszewski, M., & Nakaoka, S. (2014). A global surface ocean fCO_2 climatology based on a feedforward neural network <https://doi.org/10.1175/JTECH-D-13-00137.1>. *Journal of Atmospheric and Oceanic Technology*, *31*, 1838–1849.